Journal of Geosciences and Geomatics, 2020, Vol. 8, No. 2, 58-75
Available online at http://pubs.sciepub.com/jgg/8/2/2
Published by Science and Education Publishing
DOI:10.12691/jgg-8-2-2

Mineral Chemistry and Descriptive Petrology of the Pan-African High-K Granitoids and Associated Mafic Rocks from Mbengwi, NW Cameroon: Petrogenetic Constraints and Geodynamic Setting

Benoît Joseph Mbassa[1,*], Emmanuel Njonfang[2], Caroline Neh Ngwa[1], Michel Grégoire[3], Zénon Itiga[4], Pierre Kamgang[5], Mfomou Ntepe[1], Jesús Solé Viñas[6], Mathieu Benoit[3], Jacques Dili-Rake[1], Ferdinand Mbossi Eddy[1]

[1]Institute for Geological and Mining Research, Branch for Geophysical and Volcanological Research, P.O. Box 4110, Yaoundé Cameroon
[2]Higher Teacher Training College, University of Yaoundé I, P.O. Box 47, Yaoundé, Cameroon
[3]Géosciences-Environnement-Toulouse, UMR 5563, Université Paul-Sabatier, 14 avenue Édouard-Belin. 31400 Toulouse, France
[4]Department of Earth Sciences, University of Douala, P.O. Box 24157, Douala, Cameroon
[5]Department of Earth Sciences, University of Yaoundé I, P.O. Box 812, Yaoundé, Cameroon
[6]Instituto de Geología, Universidad Nacional Autónoma de México (UNAM), Cd. Universitaria, Coyoacán, 04510 Cd. de México, MEXICO
*Corresponding author: benjo_mbassa @yahoo.fr

Received May 30, 2020; Revised June 22, 2020; Accepted July 01, 2020

Abstract The Mbengwi Pan-African high-K calk-alkaline I-type plutonic rocks consist of granitoids and monzodiorites. These granitoids have a rather homogeneous mineralogical composition made up of calcic amphiboles, ferromagnesian and lithio-aluminous micas, quartz, feldspars, oxides, titanite and incidentally of sulphides, magmatic epidote, apatite, zircon, chlorites and carbonates. Plagioclase compositions range from Na-albite to andesine. Micas are Mg-biotite in monzodiorites and Mg-biotite, Fe-biotite, siderophyllite, lepidomelane, muscovite and phengite in granitoids. Magmatic amphiboles are made up of Fe-hornblende, Mg-hornblende, Fe-edenite, Mg-hastingsite or edenite whereas post-magmatic amphiboles are actinolite. Trace elements analyses reveal: i) low rare earth elements content in monzodiorites (average = 199.9 ppm) compared to granitoids (average = 404.65 ppm); ii) a weak to strong fractionation ($(La/Lu)_N$ = 4.5 - 102.96), iii) an enrichment in LILE and LREE relative to HFSE and HREE, and iv) negative anomalies in Rb, K, Sr, Ti, Eu and positive ones in Th and La. Mineralogical and whole rock geochemical results reveal that magmas were produced by vapor-present partial melting of one or several heterogeneous igneous protoliths relatively rich in potassium. The investigated rocks were emplaced between 4 and 34 km deep, at pressure ranging from 1.2 to 9.4 Kbars and were not subjected to post-magmatic alterations according to their Zr/Hf values (> 20). Their differentiation process is the combined result of fractional crystallization and multiple mixing and mingling.

Keywords: *Mbengwi, Northwest Cameroon, Pan-African, minerals chemistry, geochemistry*

Cite This Article: Benoît Joseph Mbassa, Emmanuel Njonfang, Caroline Neh Ngwa, Michel Grégoire, Zénon Itiga, Pierre Kamgang, Mfomou Ntepe, Jesús Solé Viñas, Mathieu Benoit, Jacques Dili-Rake, and Ferdinand Mbossi Eddy, "Mineral Chemistry and Descriptive Petrology of the Pan-African High-K Granitoids and Associated Mafic Rocks from Mbengwi, NW Cameroon: Petrogenetic Constraints and Geodynamic Setting." *Journal of Geosciences and Geomatics*, vol. 8, no. 2 (2020): 58-75. doi: 10.12691/jgg-8-2-2.

1. Introduction

Granitoids, commonly known as the major components of the continental crust, are mainly associated with syn-collisional orogenic settings. Several petrogenetic models of granitoids have been evidenced including: (1) the partial melting of crustal rocks [1,2]; (2) mixing and/or mingling of mafic mantle melts and crustal felsic magmas [3]; and (3) differentiation of primary juvenile mantle-derived material [4,5]. The post-collisional magmatism typically generated after lithospheric thickening involves variable sources, with voluminous intrusions of metaluminous/peraluminous granitoids up to alkaline-type series, and may represent a powerful tool to deliver information on crustal processes and compositions [6]. In Cameroon, this magmatism is of great interest not only to decipher the post-Pan-African crustal evolution but also the breakup of the Western Gondwana

supercontinent. Although we can mention some few studies such as the geological reconnaissance work carried out by [7] and [8] indicating the predominance of syn-tectonic potassic calc-alkaline granites and the recent specific studies done by [9,10], no thorough research work focused on the genesis of granitic rocks has yet been carried in our studied area. Therefore, new minerals chemical data, bulk rock major and trace elements contents and Sm-Nd isotopic data of the Mbengwi plutonic rocks are capitalized in this paper in order to i) constrain their geodynamic setting and ii) discuss their petrogenetic conditions.

2. Geological Framework

The Pan-African fold belt in Cameroon (Figure 1b) includes three domains [11] i) the southern domain made up of Pan-African meta-sedimentary units [12] which was thrusted onto the Archaean Congo craton towards the South [13]; ii) The central domain, located between the Sanaga fault and the Tcholliré-Banyo fault, comprises the Adamawa fault and other anastomosed faults, which constitute the Central Cameroon Shear Zone (CCSZ); and iii) The northern domain which has been affected by at least two magmatic episodes: the earlier (640- 620 Ma) corresponds to pre- to syn-tectonic calc-alkaline granitoids and the younger (≈ 580 Ma) to late tectonic granitoids [14]. The tectonic evolutionary models of the Pan-African belt in central and southern Cameroon involve an initial extension responsible of the emplacement of early Neoproterozoic sedimentary basins followed by subduction and collision between the Saõ Francisco-Congo craton, the West African craton, and the Saharan metacraton at 600 Ma [15,16], or between the Congo craton and the Saharan metacraton [17]. The resulting structures include the N70E shear zones underlined by the CCSZ, the Sanaga fault (SF) and the granulitic and migmatitic thrust sheets overriding the Congo craton [18]. Three successive tectonic events related to Pan-African collision and post-collision evolution, have been identified in Cameroon by [19] i) crustal thickening (630-620 Ma); ii) left lateral wrench movements (613-585 Ma) and iii) right lateral wrench movements (585-540 Ma) mainly marked by the CCSZ. According to their respective periods of emplacement, three main plutonic massifs have be distinguished by [20]: 1) the early pre-to syn-D_1 diorite-granodiorite strips, 2) the mostly syn-D_2, syn-kinematic porphyritic and fine-grained granites, enclosing mafic and intermediate intrusions, and 3) the late Ediacaran-Cambrian post-kinematic subcircular alkaline granitoids.

The Mbengwi area, geographically bounded by latitudes 6°06′ and 5°58′ North and longitudes 9°57′ and 10°06′ East (Figure 1c), is located in the northern domain of the Pan-African fold belt in Cameroon. The studied area consists of a Pan-African basement rocks partially covered or intruded by recent alkaline formations dated at 28.2 Ma [21]. The alkaline rocks represent a bimodal series ranging from basanites to rhyolites with a gap between 50 and 62 wt% of SiO_2. The calc-alkaline Pan-African rocks typically of I-type, are metaluminous to slightly peraluminous, displaying high-K to shoshonitic features. They result from melting of the lower continental crust with variable contribution of the oceanic crust [9].

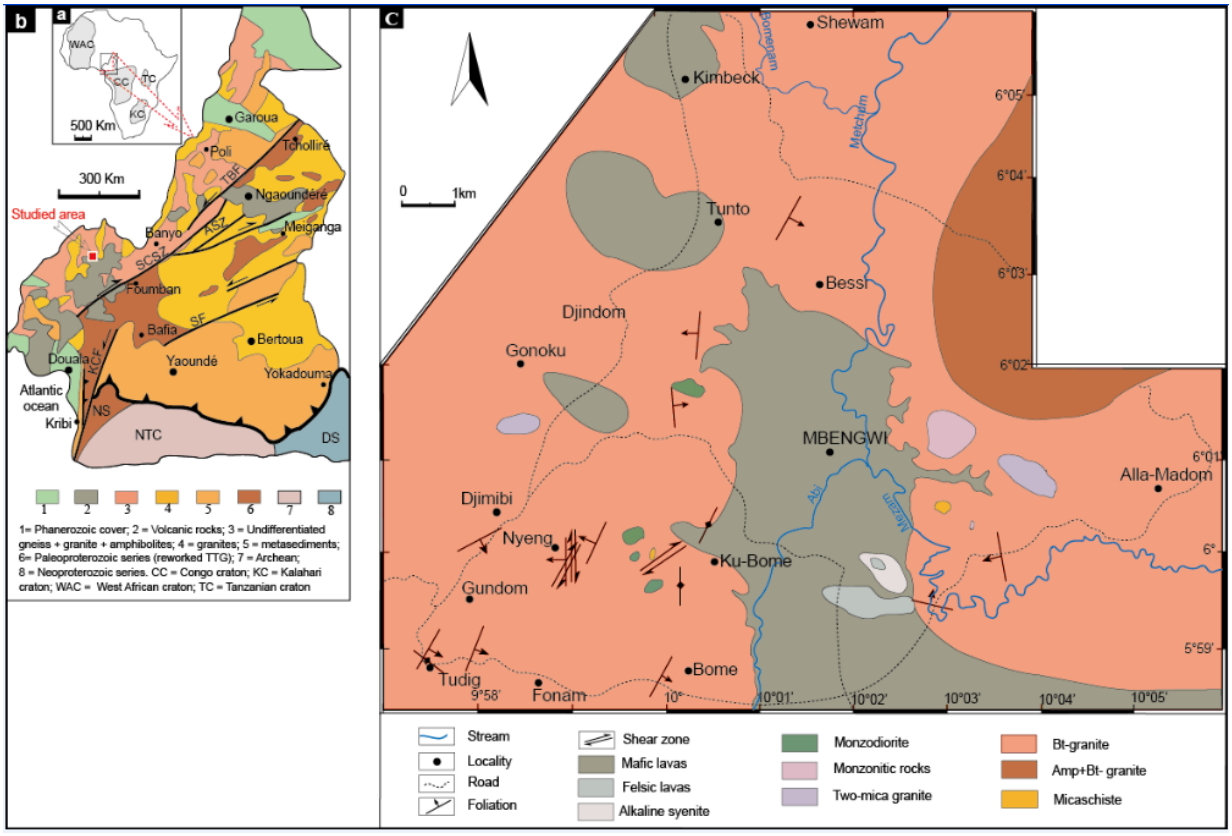

Figure 1. Geological setting of the studied area; a) location of Cameroon in Africa; b) Simplified geological map of Cameroon showing the main Pan-African domains. AF=Adamawa fault. SF=Sanaga fault. TBF= Tcholliré-Banyo fault. CCSZ= Central Cameroon shear zone. NT=Ntem complex; DS= Dja series; NS= Nyong series. 1= southern. 2= central domain. 3= northern domain; c) Geologic sketch map of the studied area

3. Sample Materials and Analytical Methods

3.1. Sample Collection and Specimen Preparation

Thirty two (n = 32) fresh rock samples of plutonic rocks were collected from various lithology, and all of them were prepared at *Geosciences Environnement Toulouse*, University of Toulouse 3 (France).

For petrographic observations and mineralogical analyses, standard-sized 27 × 46mm polished thin slices were prepared following standard procedures. 25 x 40 mm sections of rock material were mounted with epoxy on carrier glass, lapped with carborundum paper up to 2000 mesh to ~30 µm, and finished with diamond pastes 4-2-1-0.25µm on a cloth to achieve a mirror finish. Then after, they were coated with ~50 nm carbon prior to electron-probe micro-analysis to minimize charging in the electron beam.

For geochemical analyzes, rock powders were also obtained following standard processes. About 2kg of a rock sample collected from the field and initially cleared of its weathered parts is comminuted in a Tungsten jaws crusher to less than (<) 0.5cm, introduced into an agate mortar (previously cleaned with sea sand, water, alcohol and then dried with compressed air) and hosted into the SIEBTECHNIK brand mill for 12 minutes to obtain a fine powder. The powders obtained were then homogenized and split by a RETSCH cone-and-quartering then stored in hermetically sealed bottles for the geochemical analysis.

3.2. Analytical Methods

3.2.1. Mineral Main Element Chemistry

Mineral main element composition was determined using carbon-coated thin sections in a CAMECA S X 50 Electron probe micro analyzer of *Geosciences Environnement Toulouse*. The analytical conditions were 15 kV accelerating voltage and the beam size was 2×2 µm under 10 or 20 ηA, according to the resistance of the mineral to the electronic beam. Acquisition times were 10s for the peak, and 5s on both sides of the peak, for an analyzed volume of 5 μm^3. Kα lines were used. Raw main and trace elements data were ZAF-corrected using the PAP-algorithm of [22].

3.2.2. Bulk Rock Major and Trace Element Geochemistry

Major elements and trace elements were analyzed by X-ray fluorescence spectrometry (XRF) at the *École des Mines de St-Étienne* (France) and at ALS Minerals Laboratory of Sevilla (Spain) using inductively coupled plasma-optical emission spectrometry (ICP-OES) and mass spectrometry (ICP-MS) respectively. The precision of bulk rock main elements measurements performed was usually better than 1% for both SiO_2 and TiO_2, 2% for Al_2O_3 and Fe_2O_3, and better than 4% for the other major oxides. The Standard deviation for trace elements analysis was typically below 2 wt%, 0.92 wt% for SiO_2, 326.6 ppm for TiO_2, 0.45 wt% for Al_2O_3, 0.09 wt% for Fe_2O_3, 75.55 ppm for MnO, 0.14 wt% for MgO, 0.26 wt% for CaO, 0.19 wt% for Na_2O, 753.10 ppm for K_2O and 249.50 ppm for P_2O_5. Regarding bulk rock trace element determinations, calibration was performed using international reference samples (some of which were also run as unknowns in order to determine accuracy and detection limits). Mean accuracies were generally better than 5%, and the detection limits for trace elements range from 0.01 ppm (REE) to 20 ppm (Zr).

For X-ray fluorescence analysis, pressed pallets of rock samples were prepared by mixing carefully 4.5g of homogenized sample (powered to <200 mesh ASTM size) with 0.3g wax ($C_{18}H_{36}O_2N_2$) as additive binder. The mixture was pressed by applying a 200 kN force to get a uniform disk of 40 mm diameter over boric acid backing in an aluminum cup. For ICP-MS), 0.1 g of <200 mesh size powdered sample was fused with a mixture of 0.15g lithium tetraborate (flux) and 0.15g of anhydrous lithium metaborate (flux) in a same Pt container. The cold mass was taken into solution with 25 ml of 8% HNO_3 then the solution was taken in 250 ml volumetric flask and made the volume up to 250 ml maintaining 4% HNO_3 medium and 10 ppb In. In XRF and ICP-MS analyses, standard reference materials W-2A [23] and GSD-7 [24] were run under the same conditions to check analytical accuracy.

3.2.3. Sr and Nd Isotopic Analyses

Sr and Nd isotopic measurements were eluted after HF/HNO_3 digestion using Eichrom Sr-Spec, Thru-Spec and Ln-Spec resins. The measurements were performed on a Finnigan 261 multicollector thermal-ionization mass spectrometer. Sr isotopic ratios were corrected for mass fractionation with normalization to $^{86}Sr/^{88}Sr$ = 00.1194. Replicate analyses of the NBS 987 standard yielded an average $^{87}Sr/^{86}Sr$ value of 0.710255±0.00002. Nd isotopic data were corrected for mass fractionation by normalization to ratio $^{146}Nd/^{144}Nd$ = 00.7219. Replicate analyses of the La Jolla Nd standard yielded an average $^{143}Nd/^{144}Nd$ value of 0.511850±0.00001.

4. Results

4.1. Field Data and Petrography

Three main lithology types are observable: granitoids, mafic intrusions and incidentally micaschists. The studied granitoids (monzonite, Qz-monzonite, granodiorite, and granites) are medium- to coarse-grained while the mafic enclaves (monzodiorites) are microgranular. The granitoids are almost ubiquitous and mostly occupy high altitudes. They outcrop either as decametric to hectometric slabs (Figure 2a) as elongated massifs, as domes (Figure 2b), or as metric boulders of variable shapes (Figure 2h). These granitoids are locally intersected by various veins and usually enclose mafic intrusions.

Many kinematic markers such as foliation, schistosity, shears, stretching lineations, fractures and folds are perceptible on granitic rocks. Two types of foliations were identified: i) a gneissic foliation materialized by a rough alternating of light quartzo-feldspathic and dark

ferromagnesian layers and ii) a granulometric or textural-type foliation due either to the succession of parallel aplitic veins within the medium to coarse grained granite, or to an alternating pegmatitic layers and medium-grained granite (Figure 2c). The schistosity, globally oriented N-S is outlined by the alignment of micas flakes into the foliation planes or by the stretching of quartzo-feldspathic ribbon boudins conferring them an eyed appearance. This schistosity is locally internal, and rather oblique to the boudins stretching (Figure 2e). Shears are sinistral or dextral, non-coaxial, and tend to reorient the internal structures (Figure 2d). They are responsible of the formation of tension veins. The folding is evidenced by the presence of aplitic folded veins within porphyritic granitoids and the twisting of quartzo-feldspathic boudins (Figure 2f and Figure 2g) while faults are observable on the quartzo-feldspathic veins (Figure 2i).

At microscopic scale, the studied rocks are mainly characterized by a mylonitic structure, reflected by the presence of quartz (Qz) and feldspars (Fsp) megacrysts molded by microcrystals (Qz, Fsp, and mafic minerals). Three crystal sizes are identifiable: large (>1 mm), medium (1-0.5 mm), and small (≤0.4 mm) crystals. The primary mineral assemblage consists of amphibole (Amp), biotite (Bt), alkali-feldspar (Afs), plagioclase (Pl) and Qz.

In granitoids quartz appears both as interstitial anhedral fine grains usually filling cracks affecting Fsp or Amp and as medium to coarse grains. The phenocrysts are generally recrystallized with undulating extinction and often enclose Pl, Bt or Afs.

Plagioclases are tabular-shaped, often zoned and frequently display bent twin lamellas and deformational kink bands or cross twinning in some granites. The less developed crystals are usually included in Afs while the phenocrysts often enclose Amp, Bt, chlorite (Chl), opaque minerals, zircon (Zrn) or apatite (Ap). Afs are anhedral to subhedral and exhibit distinct cross-hatched and Carlsbad twins in some granites. The megacrysts show a dusty surface due to alteration and are poekilitic (pyrite + Bt + Zrn + opaque minerals + Pl + Ap) with frequent spark perthites and myrmekites.

Amp has subhedral to anhedral habit and is mostly from 0.7 x 1.5 to 0.1 x 0.3 mm in size. Crystals are generally pleochroic brown to green or bluish, frequently zoned, and some crystals have corroded margins. Microcrystals are interstitial while the phenocrysts commonly include Bt, Ap and opaque minerals.

Bt occurs as brown or greenish fine flakes, displaying a regular longitudinal cleavage. Fine crystals are interstitial or included in Fsp while phenocrysts commonly enclose Ap, Zrn, and opaque minerals. Muscovite (Ms) and phengite (Ph) crystallize at the expense of Amp in two-mica granites and appear as elongated flakes frequently cleaved and regularly included in Afs.

Figure 2. Some field observations of the studied rocks: a): Slab-shaped granitoid; b) Dome outcropping; c): textural or granulometric foliation; d): Sinistral shear: e): symetrical boudin, parallel to the foliation but with an oblique internal schistosity suggesting a dextral motion; f): fold illustrated by a flexure of a granite vein; g) fractured tension vein; h - i): Normal fault observed in a granite boulder (the direction and the amplitude of the displacement are perceptible on the quartzo-feldspathic vein)

The accessory phase consists of opaque minerals, titanite (Spn), Ap, Zrn and prehnite (Prh). Opaque minerals generally appear as rounded, angular or skeletal grains, preferentially concentrated in the interstitial microcrystalline phase or included in Fsp, Bt or Amp, Qz or Spn. Phenocrysts enclose zircon and apatite and probably resulted from Spn and Bt alteration. Spn is euhedral to subhedral in shape and occurs as frequently zoned phenocrysts or as inclusion in Fsp. Zrn is acicular, polygonal, cubic to rounded, shaped and frequently included in opaque mineral or Bt. Ap has elongated to hexagonal shape or occurs as prismatic to acicular microcrystals mostly included in spinel (Spl), Bt and Fsp. Brown or green interstitial epidote (Ep) is restricted to some granites. Prh crystallizes as interleaving lenses within Bt or Ms. Due to late alteration processes, Bt is locally replaced by Chl, Amp by Chl, Ep or calcite (Cal), iron-oxides by goethite, while sericite needles crystallized at the expense of Fsp.

4.2. Mineral Chemistry

4.2.1. Feldspars

Selected analyses of feldspars correspond both to Afs and Pl in the Or-Ab-An ternary diagram (Figure 3). Alkali feldspars compositions range from Ab to Or in almost all the granitoids except in one sample of two-mica granite (E_{145}) where only Ab is found. Pl compositions range from andesine to oligoclase in monzonites; andesine to Ab in Qz-monzonites; oligoclase in granodiorites; oligoclase to Ab in Amp+Bt- granites, Bt-granites, two-mica granites (with dominance of oligoclase) and in the leucocratic granite (with high proportion of albite). In monzodiorites Afs is Or, while Pl are more calcic than those found in granitoids with compositions ranging from oligoclase to andesine with labradorite ($An_{53.9}$) in the core.

The Fsp compositions evolution during the differentiation is characterized by: 1) an overall decrease of CaO, Al_2O_3, increase of Na_2O, and rather constant K_2O in plagioclase series; and 2) little decrease of K_2O coupled with an increase of Na_2O contents of Afs. The plagioclase zoning observed is marked by a reduction of Ca contents from the core to the rim of crystals. This depletion commonly ends in some crystals by a compositional evolution from andesine at the rim to labradorite in the core (e.g. E_{63}), or from andesine in the core to oligoclase at the rim of crystals (e.g. E_{127}). However, a reverse evolution marked by an increase of the Ca contents from the core to the rim is also observed in some crystals. A significant change in K_2O and Na_2O contents in Afs on either both sides of macle plane, or from the core to the rim of the crystals is also noticed.

4.2.2. Micas

The analyzed micas belong to the Fe-Mg and Li-Al series according to [25].

The Mg-Fe series is made up of: i) Mg-Bt in monzodiorites, monzonites, Qz-monzonites, granodiorites, and Bt-granites; ii) Fe-Bt in Qz-monzonites, Bt-granites, Amp+Bt-granites and two-micas granites; iii) siderophyllite in two-micas granites and iv) lepidomelane in Amp+Bt-granites (Figure 4a-c).

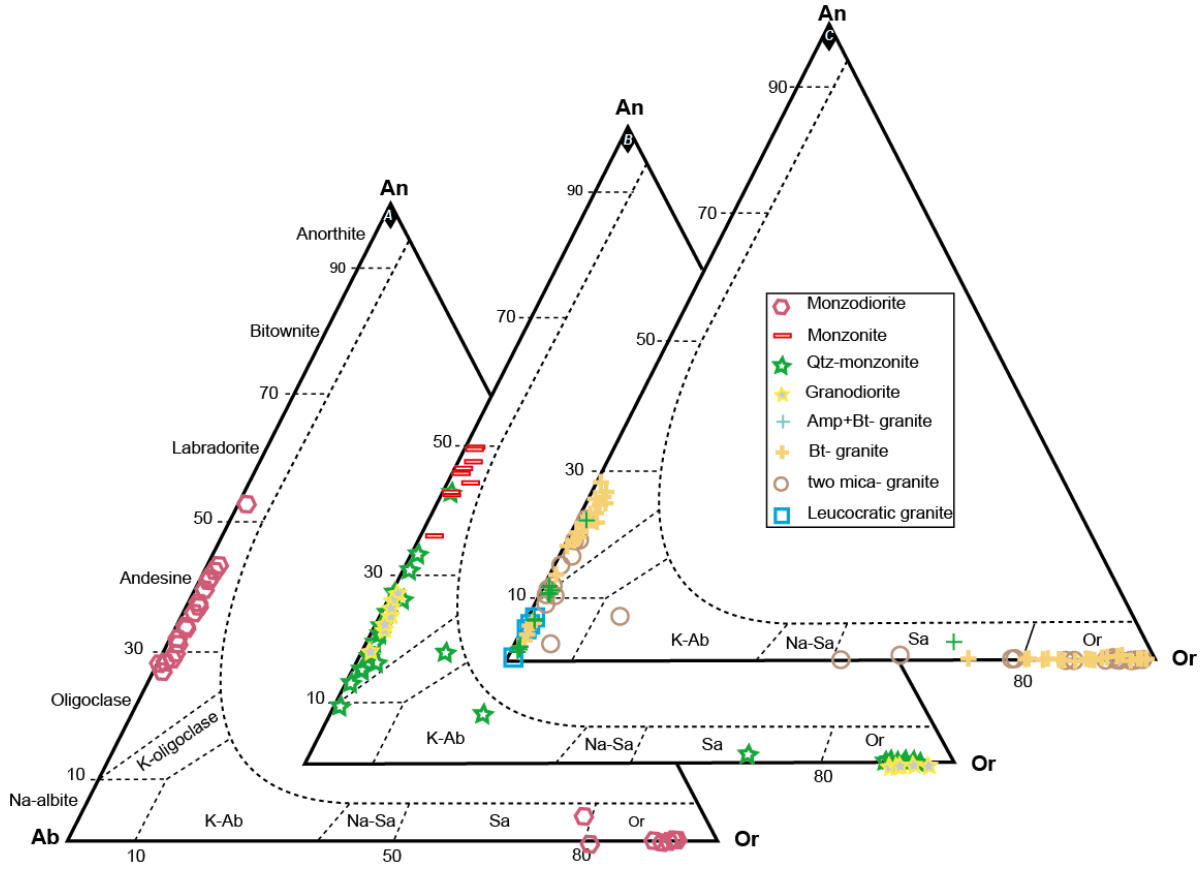

Figure 3. Ternary plots of feldspars compositions from Mbengwi plutonic rocks after [73]. (a) feldspars from monzodiorites, (b) feldspars from intermediary granitoids, and (c) feldspars from granites

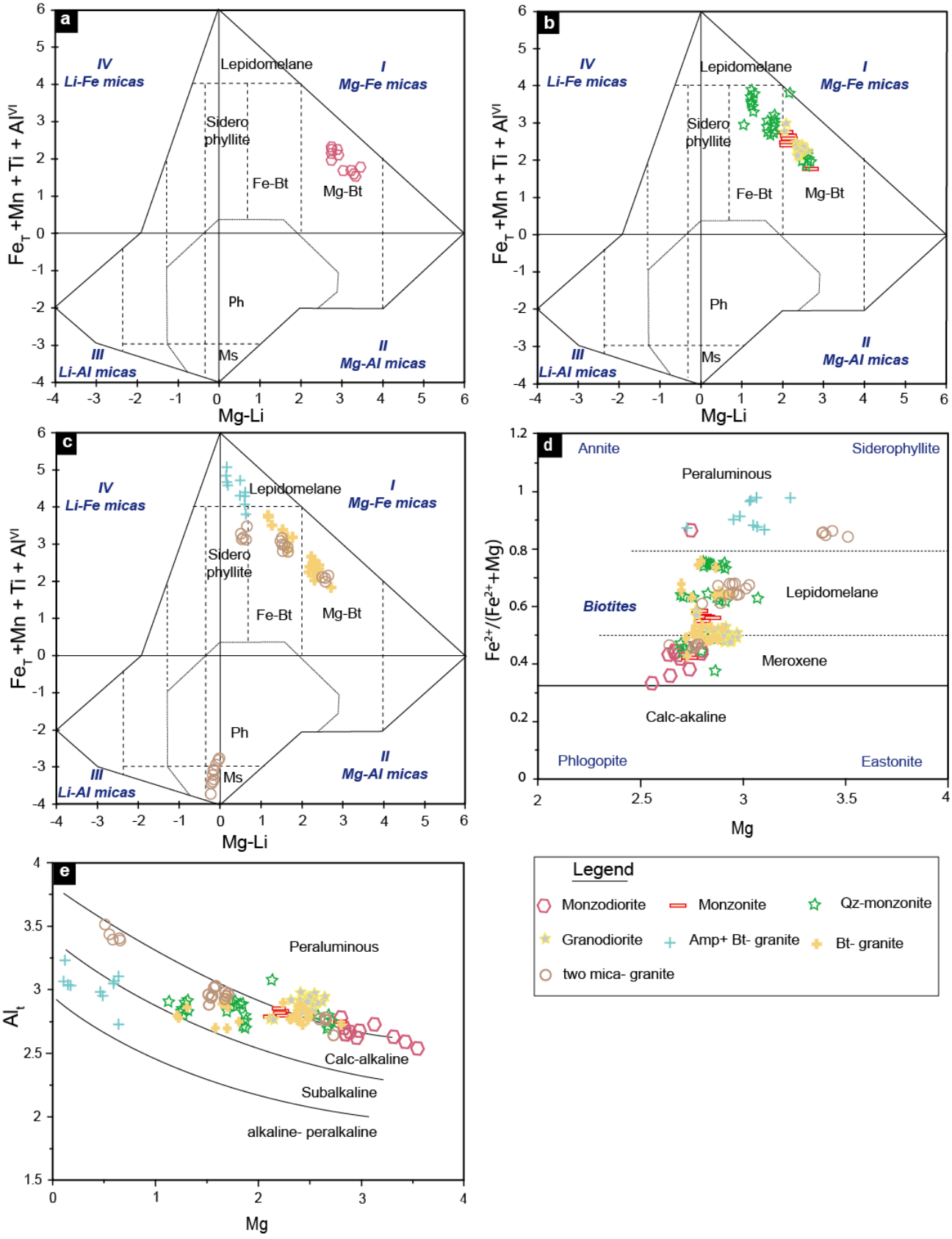

Figure 4. Plot of the micas from Mbengwi in the (Mg - Li) vs (Fe^t + Mn +Ti-Al^{IV}) discriminating diagram of [25] *(a - c)*; *(d)* the Fe^{2+}/(Fe^{2+} + Mg) vs. Al$_{total}$ (a.p.f.u.) coordinates of the Ann - Phl - siderophyllite - Eas quadrilateral. Tetrahedral micas are subdivided after [26] and [27]; and (e) the Al_2O_3 vs. MgO tectono-discriminating diagram of [74]. The Li contents in (a - c) were computed using the equation $LiO_2 = 0.289SiO_2 - 9.658$ [25]. Discrimination trends of Bt in (d) from calc-alkaline and peraluminous granitoids are after [74]. Symboles are after [75]

In the X_{Fe} vs. Al^T variation diagram of [26] completed by [27] (Figure 4d), micas from granitoids plot within the fields of Fe-poor Bt (meroxene), lepidomelane and peraluminous micas while those from monzodiorites mainly occupy the field of meroxene. The micas $FeO_T/(FeO_T+MgO)$ ratio ranges between 0.47 and 0.61 in monzodiorites and from

0.57 to 0.99 in granitoids. XMg varies from 0.39 to 0.52 in monzodiorites and ranges between 0.01 and 0.43 in granitoids. The Al_T contents gradually increase from meroxene (average: 2.80 a.p.f.u.) to peraluminous micas (average: 3.12 a.p.f.u.). The studied Bt mostly have typical compositions of calc-alkaline environments (Figure 4e) and the use of the TiO_2 - Fe*O(FeO + MnO) -MgO ternary diagram of [28] (not shown) led us to distinguish primary Bt mainly present in granites from late-magmatic Bt found in monzodiorites and some monzonites.

Li-Al micas are found only in granites and include both Ms and Ph. Muscovites compositions are characterized by X_{Fe} and Na/(Na + K) ratios ranging from 0.72 to 1 and from 0.02 to 0.1 respectively. Compared to Ms, Ph crystals are poor in Al_2O_3 (30.72-30.75 wt%), and rich in MgO (0.97-1.07 wt%) and FeO (4.34-4.26 wt%).

4.2.3. Amphiboles

The plot of selected compositions of Amp in the discrimination diagram of [29] (Figure 5a) confirms that almost all of the analyzed Amp are of magmatic origin. According to the classification scheme of [30] the studied amphiboles belong to calcium amphibole subgroup. They are characterized by a large range of Mg# [100 Mg/(Mg+Fe^{2+}): 1.81-81.70], with Si between 6.05-7.92 a.p.f.u, and total alkali contents ranging from 0.01 to 0.81 a.p.f.u. Primary amphiboles are composed of Mg-hornblende in monzodiorites, monzonites, Qz-monzonites, granodiorites and granites and pargasite in monzodiorites, Qz-monzonites, granites and rarely in monzonites. Amphibole with tremolite composition found in a monzodiorite is post magmatic field (Figure 5b). The overall evolution of amphiboles composition both in the granitoids and monzodiorites involves a decrease of MgO, CaO, and SiO_2, in addition to an increase of FeO, Al_2O_3, MnO, and K_2O contents.

4.2.4. Accessory and Secondary Minerals

Opaque minerals are mainly oxides and incidentally pyrite. In granitoids, the Fe-Ti oxides include magnetite (Mag), ilmenite (Ilm), hematite (Hem) and more rarely rutile (not shown), whereas Mag and Ilm are found in monzodiorites. All magnetite crystals are chemically characterized by lower TiO_2 contents (TiO_2 < 1.7 wt%), negligible Cr_2O_3 (< 0.2 wt%); YFe^{3+} [100Fe^{3+}/(Fe^{3+}+Cr+Al)] ratios ranging from 99.55 to 100; $Fe^{2+}{}_{\#}$ [100Fe^{2+}/(Fe^{2+}+Mg): 99.35 - 100]; Mg/Fe^{2+} (≤ 0.005); Mg# (≤ 0.20), and Fe^{3+}/(Fe^{3+} + Fe^{2+}) from 0.65 to 0.67. Ilmenite is richer in MnO (2.3-8.2 wt%) than magnetite (<0.6 wt%) or hematite (<0.3 wt%). All the analyzed Hem encompass very low apparent SiO_2 (<0.2 wt%).

Titanite chemical compositions are characterized by X_{Al} [Al/(Ti+Al+Fe^{3+})] and X_{Fe3+}[Fe^{3+}/(Ti+Al+Fe^{3+})] ratios ranging from 0.03-0.26 and 0.01-0.06, respectively. Spn crystals found at Mag rims or crystallized at Bt-ilmenite contacts are the most depleted in Ti, the most aluminous and frequently, the most calcic. Some Spn crystals exhibit euhedral shape reflecting their magmatic origin, although their Al_2O_3 contents (0.85-6.87 wt%) are of secondary Spn according to [31].

Epidotes have a composition of pistacite with [100Fe^{3+}/(Fe^{3+}+Al)] ratio varying from 25.8 to 31.6. They are rich in Al_2O_3, FeO and CaO with negligible amounts of TiO_2 (< 0.2 wt%), Cr_2O_3 and Mn_2O_3.

Chlorites compositions include ripidolite, picnochlorite and diabantite according to the classification chart of [32] (not shown). They can be considered as iron-rich (X_{Fe}: 1.22-2.74) with Al^{IV} values ranging from 1.22 to 2.74 a.p.f.u and (Ca+Na+K) < 0.5 a.p.f.u.

Carbonates are scarce and mostly composed of calcite (97.60-98.07 wt%), although the presence of low contents of siderite (< 0.7 wt%), magnesite (≤ 0.4 wt%), and rhodochrosite (≤ 1.5 wt%) are noticeable.

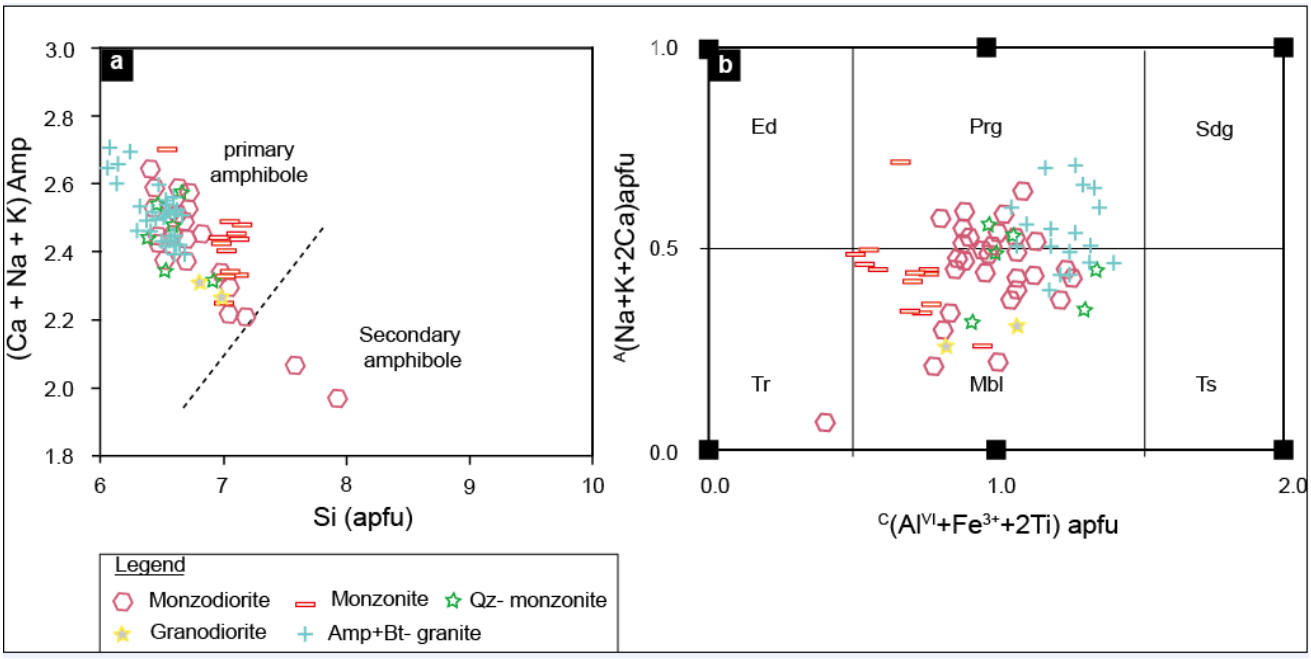

Figure 5. Amphiboles chemistry in a) the Ca+Na+K (apfu) versus Si (apfu) discriminative diagrams evaluating the primary vs secondary trend of Amp from Mbengwi rocks after [29]; b) the $^{C}(Al^{VI}+Fe^{3+}+2Ti)$ vs $^{A}(Na+K+2Ca)$ diagram, following the terminology of [30]

4.3. Whole Rock Geochemistry

Bulk-rock major and trace elements geochemical analyses of representative rock samples from the studied rocks are given in Table 1. Loss on ignition is mostly lower than 2 wt%.

Table 1. Bulk-rock main element oxide (in wt%) and trace element contents (in ppm; µg·g^{-1}ug/) measured by XRF in representative plutonic samples from Mbengwi. LG = leucocratic granite

Rock type		Monzodiorite					Monzonite			Qz-monzonite					Granodiorite		
Sample	LLD	E141	E134	E131	E33	E135	E142	E63	E69b	E144	E42	E67	E64	E65	E125	E41	E54
main element oxide contents and ignition loss in weight percent [wt%]																	
SiO_2	1.0	46.58	45.77	51.83	48.5	53.36	54.08	60.8	61.4	63.6	60.5	59.73	65.82	68.22	70.42	64.48	61.81
TiO_2	0.01	1.4	1.73	1.42	1.56	1.25	1.12	1.45	0.97	0.94	1	1.41	0.49	0.46	0.34	0.65	0.61
Al_2O_3	0.20	14.67	16.28	16.87	18.71	16.5	15.89	15.86	14.49	15.01	14.98	15.48	15.57	16.17	14.39	15.18	16.23
Fe_2O_{3T}	0.4	11.06	12	10.86	10.33	8.33	8.88	6.52	7.49	3.26	7.14	6.38	3.7	3.94	2.43	5.59	4.72
MnO	0.02	0.16	0.15	0.2	0.12	0.12	0.22	0.08	0.14	0.05	0.11	0.08	0.04	0.05	0.04	0.09	0.1
MgO	0.03	8.01	6.19	6.24	3.79	3.8	5.14	1.88	2.88	1.13	1.12	1.72	0.62	0.47	0.76	1.54	1.62
CaO	0.15	9.04	8.38	8.28	6.78	6.59	5.91	4.17	5.39	2.44	3.02	3.9	1.66	1.37	1.97	3.17	3.74
Na_2O	0.02	2.86	2.97	3.35	4.59	3.78	3.97	3.54	3.06	3.56	3.89	3.6	3.44	4.27	5.57	4.72	4.39
K_2O	0.01	2.12	2.52	2.36	2.3	3.65	2.48	4.05	5.64	5.02	4.25	4.02	6.23	5.97	5.05	1.6	2.24
P_2O_5	0.01	0.51	0.2	0.31	0.51	0.66	0.39	0.41	0.17	0.33	0.29	0.41	0.15	0.11	0.11	0.27	0.24
LOI	-	1.14	1.34	0.97	0.77	0.66	0.84	0.67	0.48	0.72	1.18	0.45	0.41	0.66	0.51	0.71	1.98
SUM total		97.55	97.53	102.69	97.96	98.7	98.92	99.43	102.11	96.06	97.48	97.18	98.13	101.69	101.59	98	97.68
trace element contents in parts per million [ppm; µg·g−1]																	
Ag	1	<1	<1	<1	<1	<1	<1	<1	<1	<1	<1	<1	<1	<1	<1	<1	<1
Ba	0.5	849	660	322	1185	2010	300	1540	473	1560	1585	1720	999	937	764	259	855
Co	1	47.3	46	42.6	35	42.5	38.5	30.2	28	47	38.1	48.5	39.9	30.9	44.3	31.2	38.8
Cr	10	370	30	70	<10	10	200	10	30	<10	<10	10	<10	<10	<10	10	<10
Cs	0.01	4.54	4.76	7.14	3.56	1.48	8.25	9.55	1.17	8.12	11.55	2.82	6.02	10.15	4.17	4.53	2.14
Cu	5	39	68	37	23	238	114	6	22	15	12	13	<5	<5	<5	29	<5
Ga	0.1	21.7	21.9	24.4	26.5	22	31.9	24.7	23	26	24.9	25.5	25.2	25.3	19.6	26.4	25.5
Hf	0.2	2.6	3.1	2.2	8.3	6.4	13.6	9.9	8.1	8.6	11.3	10.6	12.3	15.3	6.7	6.1	7.1
Mo	2	<2	<2	2	<2	<2	<2	<2	<2	<2	2	<2	<2	2	<2	<2	<2
Nb	0.2	11.3	9.9	15.3	13.1	17.2	27.2	25.5	29.8	29.5	31.2	25.5	26.1	15.7	13.3	11.2	15.8
Ni	5	93	28	35	15	13	67	8	19	5	<5	6	<5	<5	<5	<5	<5
Pb	1	14	11	13	13	25	16	23	25	32	29	24	29	28	27	18	25
Rb	0.2	120	126	154	114	104.5	180.5	182.5	113	238	178	170.5	156.5	199	178.5	91.1	80
Sn	0.2	3	3	6	2	3	10	3	2	6	4	3	2	1	2	5	6
Sr	0.1	862	564	490	1040	882	346	555	195.5	683	390	600	233	166.5	272	262	540
Ta	0.1	0.6	0.7	1.1	0.7	1.4	1	1.4	2	2.9	2.1	1.4	1.1	0.3	1.3	0.8	1.4
Th	0.05	3.67	3.48	5.72	3.67	12.85	14.55	14.3	17.25	26.2	12.7	16.05	26.6	28.9	44.4	8.99	36.3
Tl	0.5	0.5	0.5	0.6	0.5	<0.5	0.6	0.8	0.5	1	0.7	0.7	0.7	0.9	0.7	<0.5	<0.5
U	0.05	0.66	1.61	1.77	0.9	4.14	4.64	3.68	3.12	7.96	4.08	2.41	2.77	4.39	2.34	1.8	5.02
V	1	246	349	246	204	189	138	72	96	57	44	72	18	9	33	76	66
W	1	22	25	39	29	56	61	78	55	206	143	179	188	151	224	114	154
Zn	5	123	122	155	142	89	216	124	152	76	124	128	86	88	43	104	113
Zr	20	69	105	64	327	238	497	404	282	295	466	430	466	580	213	218	259
Y	5	23.1	19.5	32.8	20.2	31.4	65.4	16.5	36.2	34	31.6	17.2	30.5	28.4	17.2	21.9	32.1
Rare Earth element contents in parts per million [ppm; µg·g−1]																	
La	0.5	34.8	19.4	28.1	41.9	46.9	38.7	149.5	72.7	82.4	74.1	100	166	130	45.2	29.9	62.7
Ce	0.5	70.6	42	57.6	92.6	105	93.4	227	135	183.5	141.5	177	294	285	85.5	61.3	119.5
Pr	0.03	8.16	5.11	8.1	11.6	12.05	14.1	22.3	15.85	20.3	15.85	18.45	29.6	25.3	8.49	7.11	12.65
Nd	0.1	33.8	22.7	36.8	49.1	48.1	66.3	73.3	60.9	75.7	61	65.6	102	87.3	29.6	30.2	46.5
Sm	0.03	6.87	5.09	8.56	9.3	8.86	16.7	9.68	10.85	12.2	10.5	9.64	15	13.5	5	7.02	8.67
Eu	0.03	2.04	1.56	1.9	2.65	2.79	2.36	2.4	1.01	2.3	2.43	2.27	1.42	1.41	0.97	1.37	1.52
Gd	0.05	6.46	4.88	7.76	7.71	7.93	14.4	8.51	9.88	9.74	9.13	7.74	13.15	12.15	4.56	6.34	7.86
Tb	0.01	0.95	0.75	1.21	1.04	1.18	2.28	0.91	1.45	1.14	1.29	0.91	1.63	1.52	0.63	0.9	1.18
Dy	0.05	4.73	3.95	6.49	4.7	6	12	3.64	7.29	5.02	6.27	3.76	7.16	6.8	3.24	4.38	6.24
Ho	0.1	0.9	0.75	1.23	0.75	1.16	2.31	0.63	1.4	0.97	1.17	0.65	1.27	1.19	0.62	0.82	1.19
Er	0.03	2.49	2.13	3.5	1.92	3.37	6.56	1.77	3.96	2.89	3.43	1.8	3.4	3.25	1.83	2.27	3.53
Tm	0.01	0.31	0.29	0.49	0.22	0.48	0.94	0.2	0.55	0.37	0.45	0.21	0.39	0.37	0.27	0.32	0.5
Yb	0.5	1.89	1.78	3.13	1.26	3.04	5.87	1.23	3.45	2.42	2.93	1.26	2.34	2.22	1.79	1.97	3.08
Lu	0.01	0.29	0.26	0.46	0.18	0.5	0.9	0.18	0.53	0.42	0.45	0.18	0.34	0.33	0.27	0.3	0.44
ΣREE		174.29	110.65	165.33	224.93	247.36	276.82	501.25	324.82	399.37	330.5	389.47	637.7	570.34	187.97	154.2	275.56
Zr/Hf		26.54	33.87	29.09	39.40	37.19	36.54	40.81	34.81	34.30	41.24	40.57	37.89	37.91	31.79	35.74	36.48
Eu/Eu*		0.938	0.959	0.714	0.958	1.019	0.466	0.810	0.299	0.646	0.760	0.805	0.310	0.337	0.622	0.626	0.564
(La/Yb)N		12.51	6.10	7.40	22.59	10.48	4.48	82.57	14.32	23.13	17.18	53.91	48.19	39.78	17.15	10.31	13.83
(La/Sm)N		3.16	2.05	2.38	2.81	3.31	1.45	9.64	4.18	4.22	4.41	6.48	6.91	6.01	5.65	2.66	4.52
(La/Lu)N		12.46	6.34	7.74	24.16	9.74	4.46	86.21	14.24	20.36	17.09	57.67	50.68	40.89	17.38	10.35	14.79
(Gd/Yb)N		2.77	2.01	2.22	4.95	2.11	1.98	5.60	2.32	3.26	2.52	4.97	4.55	4.43	2.06	2.60	2.06

Rock type		Amph + Bt granite					Bt-granite						Two-mica granite				LG
Sample	LLD	E68	E611	E69	E126	E129	E2	R2	E6	E12	E20	E53	E60	E62	E145	E610	E66
main element oxide contents and ignition loss in weight percent [wt%]																	
SiO_2	1.0	69.13	69.5	72.49	70.8	69.91	70.01	70.8	71.65	73.41	75.88	75.21	67.8	74.27	70.24	71.24	79.2
TiO_2	0.01	0.34	0.36	0.38	0.27	0.22	0.32	0.25	0.47	0.35	0.09	0.15	0.42	0.08	0.47	0.17	0.03
Al_2O_3	0.20	13.3	13.89	13.95	13.67	14.37	13.88	13.88	14.95	11.82	12.68	12.17	15.04	14.45	13.43	13.81	12.57
Fe_2O_3	0.4	3.68	3.68	3.75	1.9	2.2	2.3	1.61	2.02	2.27	0.62	0.68	2.91	0.87	2.69	2.08	0.24
MnO	0.02	0.06	0.07	0.07	0.03	0.03	0.05	0.04	0.03	0.04	0.01	0.01	0.04	0.03	0.03	0.06	0
MgO	0.03	0.25	0.12	0.23	0.49	0.55	0.64	0.38	0.57	0.21	0.16	0.17	0.67	0.2	0.85	0.26	0.06
CaO	0.15	0.97	0.93	0.86	1.38	1.26	1.32	1.21	1.49	0.38	1.6	0.76	1.61	0.98	1.98	0.52	0.4
Na_2O	0.02	3.8	3.22	3.75	3	3.12	3.02	3.49	4.37	2.15	3.9	2.94	3.52	4.16	3.28	3.01	2.76
K_2O	0.01	5.5	5.91	6.05	5.61	6.07	6.02	5.8	5.63	6.94	2.98	5.31	5.44	4.89	4.16	5.2	6.41
P_2O_5	0.01	0.06	0	0.05	0.08	0.08	0.11	0.09	0.14	0.02	0.02	0.02	0.14	0.07	0.15	0	0.02
LOI	-	0.38	0.4	0.35	0.35	0.32	0.76	0.57	0.67	0.23	0.75	0.31	0.54	0.55	0.81	0.8	0.27
SUM total		97.47	98.08	101.93	97.58	98.13	98.43	98.12	101.99	97.82	98.69	97.73	98.13	100.55	98.09	97.15	101.96
trace element contents in parts per million [ppm; μg·g−1]																	
Ag	1	<1	<1	<1	<1	<1	<1	<1	<1	<1	<1	<1	<1	<1	<1	<1	<1
Ba	0.5	319	233	293	1160	1175	903	1735	1220	953	313	1195	1275	797	1220	203	700
Co	1	52	36.5	56.8	55.2	47.7	53.1	50.5	51	57.1	62.1	79.3	44.7	55	57.8	46.7	81.2
Cr	10	<10	<10	<10	<10	<10	<10	<10	<10	<10	<10	<10	<10	<10	10	<10	<10
Cs	0.01	1.7	0.58	1.53	4.06	3.31	4.52	2.54	3.44	4.04	2.54	1.81	3.02	5.46	9.07	10.2	3.42
Cu	5	<5	<5	6	<5	5	10	<5	<5	<5	<5	5	<5	<5	<5	<5	5
Ga	0.1	25.4	23.1	24.1	19.9	20.1	19.4	19.3	21.2	17.3	17.5	14.6	23.6	22.2	23	26.6	22.5
Hf	0.2	15.5	18.3	16.5	5.7	11.6	5.7	5.8	8.2	12.1	2.7	2.7	7.7	2.4	6.5	2.7	11.3
Mo	2	<2	2	<2	<2	<2	<2	<2	<2	<2	<2	<2	<2	<2	<2	<2	<2
Nb	0.2	28.3	27.4	30.3	10	6.5	7.6	11.2	13.6	17.1	4	5.4	10.6	12.7	13.3	33.7	3.3
Ni	5	<5	<5	<5	<5	<5	5	<5	<5	<5	8	<5	<5	<5	<5	<5	<5
Pb	1	26	19	25	32	35	32	30	33	40	22	30	33	42	23	39	47
Rb	0.2	119.5	64.5	113.5	194.5	187.5	206	170.5	155.5	219	86.8	142	151	170	188.5	230	170.5
Sn	0.2	2	1	1	2	1	2	1	3	4	1	2	3	4	3	10	<1
Sr	0.1	78.9	62.7	71.2	366	389	314	482	341	178.5	217	368	312	177	706	73.3	398
Ta	0.1	1.4	1.1	1.5	1.3	0.7	0.6	1	0.9	2	0.8	0.6	0.6	1.3	1.4	3.5	0.2
Th	0.05	37.6	41.5	34.4	44.8	126	16.55	30.1	18.4	23.7	8.19	34.5	17.1	8.59	30	13.4	24
Tl	0.5	0.5	<0.5	0.5	0.9	0.8	0.8	0.6	0.7	0.9	<0.5	0.6	0.7	0.9	0.7	1	0.6
U	0.05	2.73	1.31	2.22	2.23	5.75	1.34	5.08	2.02	2.83	1.19	3.05	1.86	3.96	6.05	2.6	2.59
V	1	8	<5	6	23	36	23	19	9	11	5	13	18	<5	40	<5	<5
W	1	269	190	292	278	234	256	259	252	297	328	419	217	294	285	246	433
Zn	5	95	71	88	42	36	64	30	43	42	16	15	63	43	70	102	<5
Zr	20	648	809	681	186	350	191	194	303	408	73	83	291	59	219	59	250
Y	5	31.6	18.6	28.3	15.3	9.2	51.5	10.9	10.8	103	9.5	9.8	16.1	14.7	11.4	19.2	3.4
Rare Earth element contents in parts per million [ppm; μg·g−1]																	
La	0.5	284	367	242	100.5	110.5	75	79.1	110	55.6	20.6	122	114	19.9	77.8	29.3	9.7
Ce	0.5	406	661	402	156.5	258	101	147.5	177.5	96.2	18.3	189.5	183	37.7	126	54.2	13.3
Pr	0.03	50.4	66.4	43	17.3	22.4	12.1	14.55	16.35	14.4	2.73	16.45	18.75	4.16	11.5	6.37	1.12
Nd	0.1	176.5	232	151.5	57.7	73.4	42.2	50	51.8	65.2	9.5	50.8	63.6	15.5	37.9	24.1	3.6
Sm	0.03	21.1	25.4	18.95	7.91	9.74	5.98	7.1	6.24	17.8	1.52	5.91	8.76	3.38	5.55	5.43	0.76
Eu	0.03	0.78	0.61	0.63	1.18	1.17	1.13	1.37	1.08	2.68	0.64	0.88	1.32	0.68	1.16	0.38	0.11
Gd	0.05	16.9	19.7	16	6.48	7.26	6.26	5.52	5.18	21.8	1.64	5.2	7.75	3.22	4.78	5.02	0.7
Tb	0.01	1.76	1.73	1.67	0.74	0.67	0.82	0.57	0.54	4	0.24	0.52	0.85	0.49	0.55	0.75	0.12
Dy	0.05	6.78	5.41	6.75	3.12	2.27	4.65	2.32	2.16	23.4	1.17	2	3.48	2.59	2.36	3.85	0.68
Ho	0.1	1.22	0.87	1.15	0.57	0.38	1.15	0.43	0.39	4.55	0.25	0.36	0.59	0.48	0.42	0.69	0.15
Er	0.03	3.67	2.72	3.47	1.71	1.18	3.79	1.26	1.21	11.65	0.79	1.07	1.63	1.37	1.19	1.86	0.46
Tm	0.01	0.46	0.28	0.42	0.23	0.14	0.5	0.17	0.15	1.43	0.12	0.14	0.17	0.16	0.15	0.25	0.09
Yb	0.5	2.92	2.05	2.75	1.48	1.04	2.78	1.07	1.06	7.64	0.89	0.93	1.09	1.02	1.08	1.53	0.5
Lu	0.01	0.51	0.37	0.45	0.21	0.17	0.49	0.17	0.17	0.92	0.15	0.13	0.17	0.15	0.15	0.23	0.09
ΣREE		973	1385.54	890.74	355.63	488.32	257.85	311.13	373.83	327.27	58.54	395.89	405.16	90.8	270.59	133.96	31.38
Zr/Hf		41.81	44.21	41.27	32.63	30.17	33.51	33.45	36.95	33.72	27.04	30.74	37.79	24.58	33.69	21.85	22.12
Eu/Eu*		0.126	0.084	0.111	0.505	0.426	0.566	0.670	0.582	0.417	1.241	0.486	0.491	0.631	0.690	0.223	0.462
(La/Yb)N		66.07	121.62	59.78	46.13	72.18	18.33	50.22	70.50	4.94	15.72	89.12	71.05	13.25	48.94	13.01	13.18
(La/Sm)N		8.41	9.02	7.97	7.93	7.08	7.83	6.96	11.01	1.95	8.46	12.89	8.13	3.68	8.75	3.37	7.97
(La/Lu)N		57.80	102.96	55.82	49.67	67.47	15.89	48.30	67.16	6.27	14.25	97.41	69.61	13.77	53.84	13.22	11.19
(Gd/Yb)N		4.68	7.77	4.71	3.54	5.65	1.82	4.17	3.95	2.31	1.49	4.52	5.75	2.55	3.58	2.65	1.13

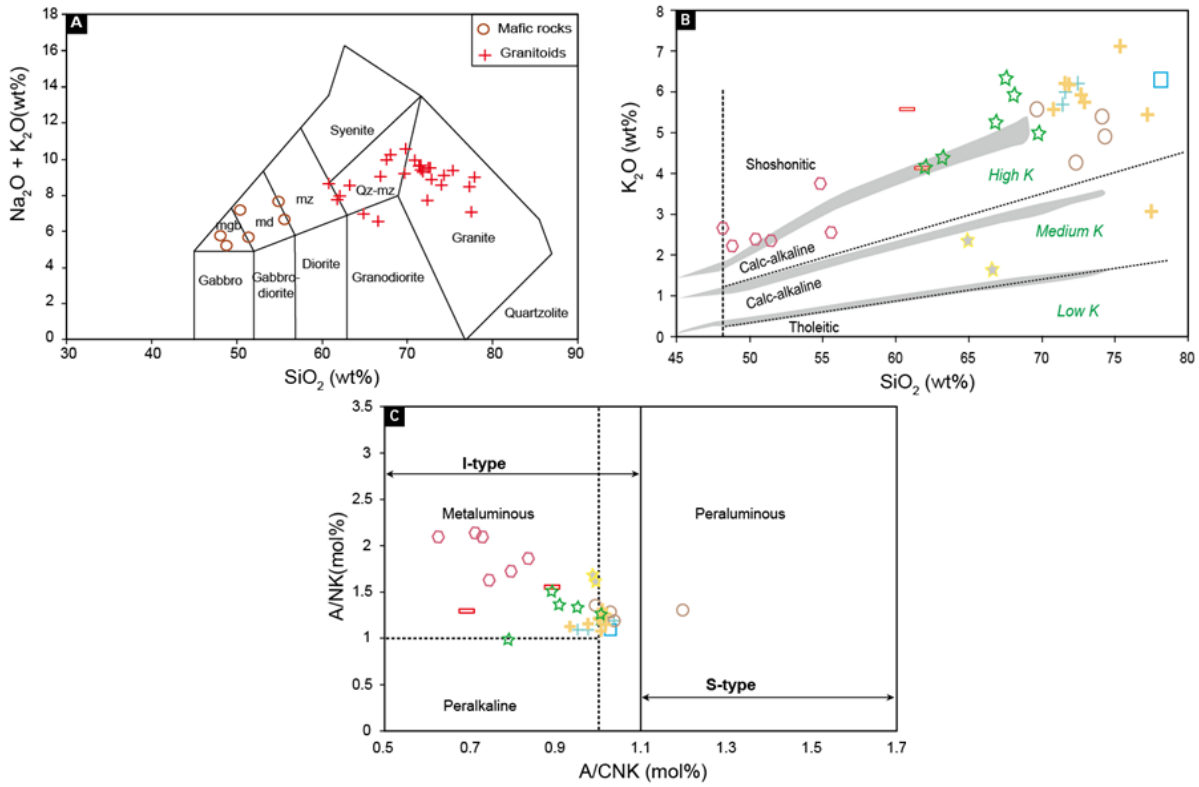

Figure 6. Chemical classification of the studied rocks in: A) the compositional TAS diagram of [33] B) K_2O vs. SiO_2 diagram illustrating the high-K calc-alkaline and shoshonitic affinities of the Mbengwi plutonic rocks. Subdivision after [35] and [76]; C) A/NK [Al_2O_3/ (Na_2O + K_2O)] vs. A/CNK [Al_2O_3/(CaO + Na_2O + K_2O)] diagram after [36]. The boundary between type-I and type-S granites is after [37]

4.3.1. Major Elements Data

In the classification diagram of [33], the mafic enclaves plot in the monzogabbro and monzodiorite fields, whereas the granitoids samples fall in the monzonite, Qz-monzonite, granodiorite and granite fields (Figure 6A). Due to both the lack of Cpx and the nature of plagioclase they have, all the samples plotting in the monzogabbro field were considered as monzodiorites.

The granitoids samples from Mbengwi area have overall high K_2O (1.7-7.1 wt%), moderate high Na_2O (2.2-5.5 wt%) and moderate Al_2O_3 (12.1-17.1 wt%) contents and low Mg# (6.1 - 40.7). Their CaO/Al_2O_3 molar ratios range from 0.06 to 0.68 and [(Na_2O + K_2O)/Al_2O_3] vary from 0.59 to 1.02. According to [34], almost all granitoids are potassic regarding their Na_2O- K_2O value (< 2) except the granodiorites. Nearly all the studied rocks plot within the high-K to shoshonitic fields in the K_2O vs. SiO_2 diagram of [35], except granodiorites and one sample of Bt-granite (E_{20}) which occupy the field of medium potassic rocks (Figure 6B). Given their position in the diagram of [36] and [37] (Figure 6C), the studied granitoids are mainly metaluminous to weakly peraluminous in composition. Only a Qz-monzonite sample containing normative acmite (E_{125}) displays a molar (Na+K) > Al and could be considered as peralkaline according to [38]. Apart from a two-mica granite sample (E_{610}) that plots in type-S (A/CNK >1.1) field, these granitoids are mostly of type I. Al_2O_3, TiO_2, Fe_2O_{3t}, MgO, MnO, CaO and P_2O_5 are negatively correlated contrary to K_2O which has a positive correlation with SiO_2 both for granitoids and associated monzodiorites (not shown).

Monzodiorites have moderate K_2O (2.2-3.7 wt%), moderatly high Na_2O (3-4.8 wt%), and high Al_2O_3 (15.4-19.4 wt%) contents. They are mainly potassic ((Na_2O-K_2O < 2) and plot within the high-K to shoshonitic fields (Figure 6B). Their CaO/Al_2O_3 molar ratios vary from 0.66-1.06 while [(Na_2O + K_2O)/Al_2O_3] vary from 0.47 to 0.62, with Mg# ranging between 42.1 and 58.9. They are metaluminous and of type I (A/CNK: 0.63-0.84) (Figure 6C).

Normative composition of monzodiorites (not shown) is marked by the lack of normative Qz alongside the occurrence of olivine (2-18.9 wt%) and nepheline (3.5-6wt%). Granitoids are characterized by i) the occurrence of normative acmite in one Bt-granite sample (E_{125}) and ii) the presence of normative corundum, except in samples containing normative diopside.

4.3.2. Trace Elements Data

The whole rock trace elements analyses of granitoids are characterized by moderate Sr (73.3-683 ppm), Y (3.4-51.9 ppm) contents and high Ba (203-1720 ppm), Rb (80-238 ppm), Nb (3.3-33.7 ppm), and Zr (73-809 ppm) contents, when compared with most I-type granitoids, and the average continental crust. The moderate Sr and high Rb contents of these rocks give rise to moderate to high Rb/Sr values (average = 0.73).

Monzodiorites exhibit high Sr (346-1040 ppm; average = 697 ppm), Rb (104.5-180.5 ppm; average = 133 ppm), Ba (300 - 2010 ppm; average= 888 ppm), Nb (9.9-27.2 ppm; average = 15.5 ppm) and Zr (64-697 ppm; average = 217 ppm), but moderate Y (19.5-65.4 ppm; average = 32 ppm) contents, compared with the average continental crust.

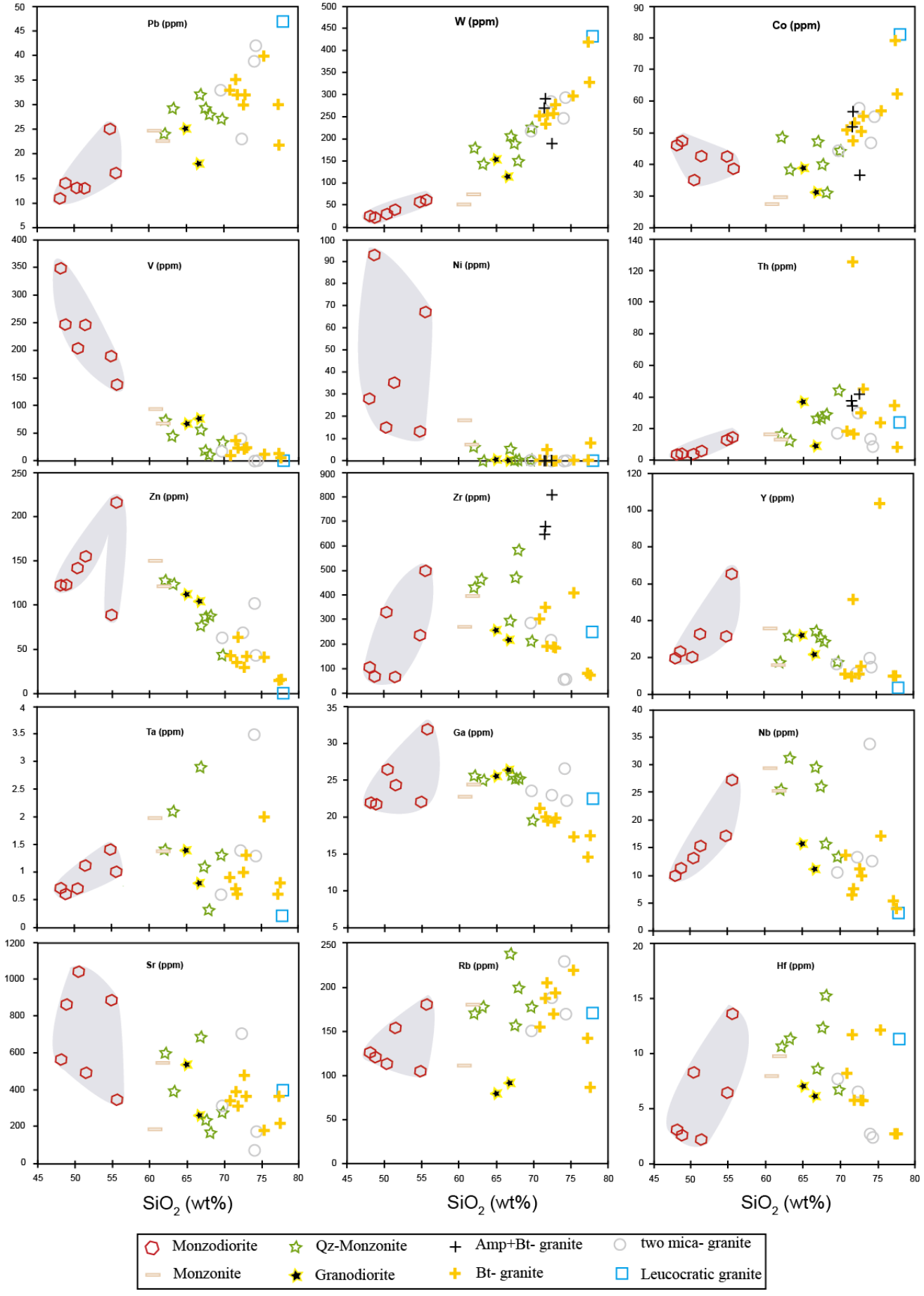

Figure 7. Harker diagram of some trace elements. The grey field includes monzodiorite samples

V, Sr and Ni show a compatible behavior over the entire range, while W, Pb and Th appear incompatible (Figure 7). Co, Zn, Y, Nb and Ta change their behavior from monzodiorites to granitoids and could be considered as transitional. Due to the marked depletion in Rb of these granitoids, their K/Rb ratios (117.2-792.7; average = 267.1) are close both to the average of magmatic rocks (230; [39]) and the chondritic values (242; [40]). The granitoids suite exhibit significantly high Rb/Sr ratios (0.14-3.14) compared to the monzodiorites characterized by rather low ones (0.11 - 0.52).

Chondrite normalized incompatible multi-element patterns of both groups (Figure 8) exhibit: i) an enrichment in almost all the analyzed elements relative to chondrite except P; ii) enrichment in LILE compared to HFSE, iii) negative anomalies in Rb, K, Ta, Sr, P and Ti; iv) positive anomalies in Th, La and Ce for all the granitoids and in Y and Tb only in few Bt-granites and Amp+Bt-granites. However, monzodiorites are less enriched in incompatible LILE and HFSE relative to granitoids.

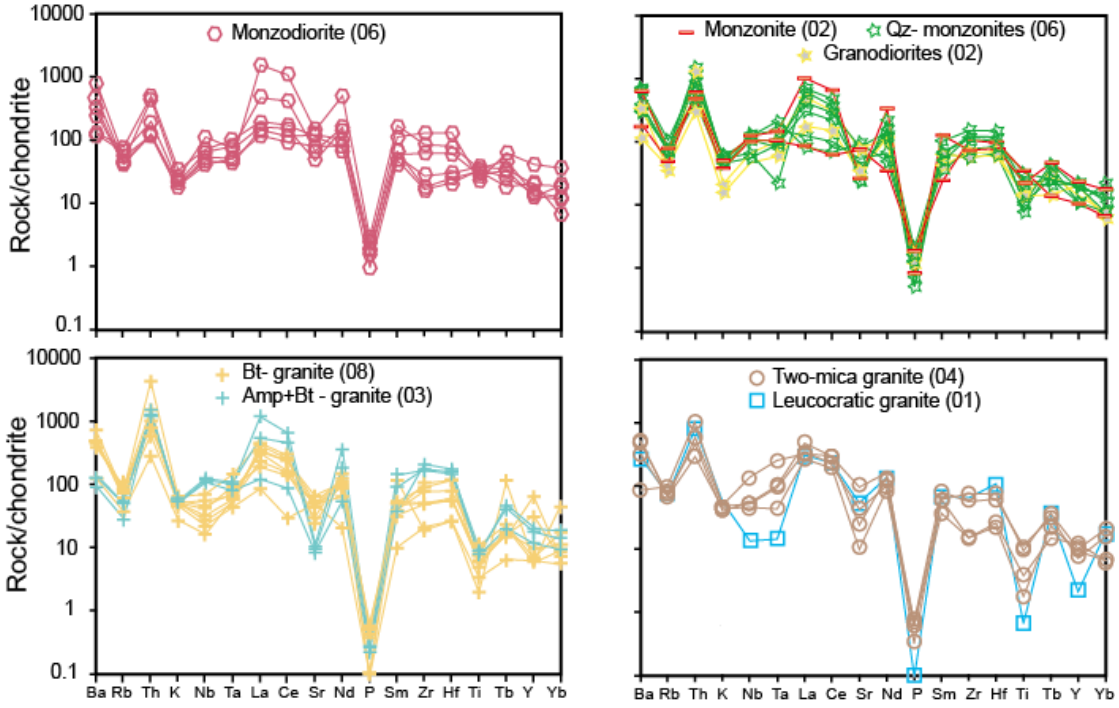

Figure 8. Chondrite-normalized multi-element diagrams using the chondrite normalizing values of [77]

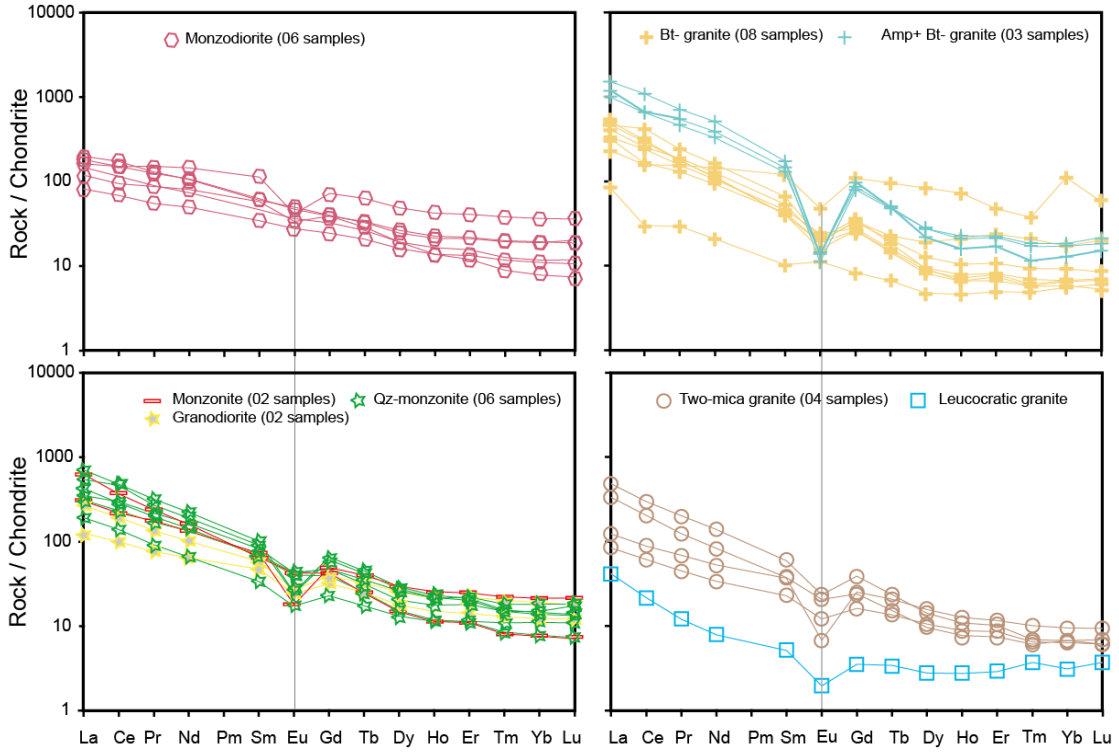

Figure 9. Chondrite-normalized REE diagrams using the chondrite normalizing values of [77]

The granitoids samples have high REE contents (average ∑REE = 232 ppm), with normalized La and Lu values ranging between 40-1548 and 4-37 respectively. The REE fractionation is more pronounced for LREE compared to HREE and the degree of LREE fractionation in granitoids (average $(La/Sm)_N$ = 6.77) is higher than the one from monzodiorites (average $(La/Sm)_N$ = 2.53). The situation differs for HREE as both granitoids (average $(Gd/Yb)_N$ = 3.64) and associated monzodiorites (average $(Gd/Yb)_N$ = 2.67) are moderately to fairly fractionated given their almost flat patterns. However, Bt-granites are strongly fractionated according to their average $(La/Lu)_N$ = 42.64 and $(Gd/Yb)_N$ = 7.75 values. Overall, both granitoids and monzodiorites display enriched, parallel to sub-parallel REE patterns, characterized by moderate to steep slopes (Figure 9) because of their enrichment of the LREE relative to middle and HREE ($(La/Yb)_N$; 4.9-121.6). The REE patterns exhibit negative Eu anomalies except for E_{20} (Bt-granite sample) with rather variable ranges (Eu/Eu*: 0.08-1.24) for granitoids and (0.46-1.02; average = 0.84) for monzodiorites.

5. Discussion

5.1. Origin of Magmas and Petrogenetic Constraints

The chemistry of granitic rocks is mostly controlled by the composition of the source. Granitoids can result either from fractional crystallization of mantle derived magma, or from partial melting of crustal rocks. Concerning the production of high-K magmas in converging tectonic environments such as the Pan-African fold belt in Cameroon, two main processes have been identified to explain: 1) in continental arc environments, parental mantle magmas enriched in fluids could be contaminated by crustal material during ascent [41]; 2) in syn- to post-collisional environments, crustal rocks could melt following decompression after peeling at the base of the lithosphere [42,43]. Compositional differences of magmas produced by partial melting of those different protoliths under variable conditions of melting are shown in Figure 10. In this diagram, several observations can be made: i) The parental magmas of the studied plutonic rocks probably originated by partial melting of meta-igneous source with a negligible contribution of a metapelite; ii) The magma of the monzodiorites, monzonites and two Qz-monzonites (E_{42} and E_{67}) derived from partial melting of amphibolite; iii) Granodiorites magmas derived from partial melting of dacite and tonalite; iv) Granites and Qz-monzonites are mostly derived from the partial melting of a metagreywacke and incidentally a metapelitic source (E_{12}, E_{68}, E_{69}).

The abundance of hydrous minerals especially Amp and Bt in monzodiorite and some granitoids, suggests that their parental magmas were relatively water-rich. According to [44], this water is probably provided by major thrust or shear zones that concentrate and channel fluids in the crust. Furthermore, the presence of Spn+ Mag + Qz paragenesis alongside amphiboles having medium to higher Mg# in addition to the very low MgO contents of Mn-ilmenite imply relatively high oxygen fugacity [45]. As stated by [42], the high-K calc-alkaline to shoshonitic and metaluminous characters of the studied rocks involve a metaluminous and relatively K-enriched source. The metaluminous to weakly peraluminous feature as well as the presence of Mag and Spn as main accessory minerals in the studied plutonic rocks suggest that their magma may have been formed by partial melting of a basic component according to [46].

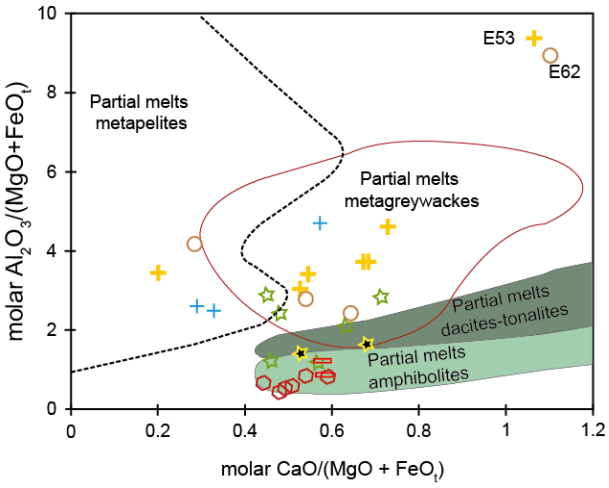

Figure 10. Plot of the Mbengwi plutonic rocks in the molar $Al_2O_3/(MgO + FeO^T)$ vs. $CaO/(MgO + FeO^T)$ [80]; The composition fields of the magmas produced by experimental melting of various sources are from [78] and [79]

5.1.1. Magma Source

Chemically, as we have mentioned before, the Mbengwi granitoids are weakly peraluminous, with high total alkali content (mostly > 8.1 wt%), low FeO^T/MgO (very few > 5) and low Mg#. The low Mg# in addition to their high-K calc-alkaline geochemical features, rule out an origin from the direct melting of a peridotitic mantle source [47], and a mixing between crust- and mantle-derived melts [48]. The crustal origin of the studied rocks already evidenced by [9] is to some extent, confirmed by Rb/Ti and Rb/Sr values. The difference in Rb/Ti ratio values of the monzodiorites (0.01-0.03; average: 0.02), and those of the host granitoids (0.2-1; average: 0.129) suggests that the rock types were derived from different magma sources according to [49]. The Rb/Sr ratios of the granitoids suite fall within a range of 0.15-3.14, with an average of 0.73; while the same ratios range from 0.11-0.52 with an average of 0.24 for monzodiorites. Such Rb/Sr ratios preclude any participation of mantle materials in the genesis of these rocks since mantle materials possess very low Rb/Sr ratios, (0.1-0.01; [39]). Therefore, the monzodiorites parental magma may probably represent non-differentiated cumulative parts of the granitoids magma.

5.1.2. P and T Crystallization Conditions

Generally, many igneous rocks lack mineral assemblages suitable for thermobarometric analysis. Either the thermodynamic variance is high, or, the phases are characterized by component exchanges easily reset during slow cooling or later thermal events. However, it remains possible to determine crystallization or emplacement temperature and pressure conditions in many granitic

intrusions through mineral equilibria less susceptible to subsequent readjustment. We have used plagioclase-hornblende thermobarometry (temperature by [50,51]; pressure by [52] and [53]) and also taken into account the total Al content of Bt to estimate the crystallization pressures for granites lacking Amp, using the equation: P (kbar) = 3.03 x Al_T - 6.53 (±0.33) from [54]. Therefore, the depth of solidification was appraised from a pressure-depth relationship of 1 kbar ≈ 3.6 km. The minimum pressure is estimated at 1.22 Kbars in a monzodiorite whereas the maximum pressure is 9.4 Kbars in Amp+Bt- granite, meaning that Mbengwi plutonic rocks crystallized at depths ranging from 4.4 to 33.8 km. The corresponding crystallization temperatures range from 764°C to 537°C in granitoids while those from monzodiorites crystallized between 789°C and 685°C.

The oxidizing or reducing nature of the magmatic environment had been deciphered using X_{Mg} ($Mg/Mg+Fe^{2+}$) values of Bt according to [55]. Biotites that crystallized under oxidizing conditions tend to show higher X_{Mg} values compared to those formed in a reducing environment [56]. The X_{Mg} of Bt from monzodiorites (0.50-0.67) are significantly higher compared to that of Bt from granitoids (0.02-0.58); and therefore, might be consistent with their moderately to strongly oxidized nature.

5.2. Magmatic Differentiation

The Mbengwi plutonic rocks show a relative large range of major and trace elements compositions, as well as Sr-Nd isotopic compositions. Several processes could therefore be envisioned to explain their genesis such as magma mixing and/or fractional crystallization.

5.2.1. Magma Mixing

In basement rocks, the process of magma mixing is commonly evidenced by the occurrence of dark enclaves of varying sizes [57]. Several field observations, petrographic feature (Figure 11a-d) in addition to mineralogical and geochemical evidences are taken into account to decipher the magma mixing.

The presence of multiple round or elliptical fine-grained melanocratic enclaves along with their chilled margins against granitoids is therefore likely a strong evidence for the involvement of magma mixing during the differentiation of the Mbengwi plutonic rocks. The change in the shape of fine-grained mafic enclaves from round to elliptical, the lack of residual minerals (e.g. andalusite, sillimanite, cordierite and garnet) in addition to their relative high hornblende and biotite contents compared to that of the neighboring host granitoids are typical signatures of enclaves formed by injections of mafic material as magma globules into the host granitic magmas during mixing process [58,59]. The contacts between enclaves and host rocks which are not clear, but chilled, are indicative of a limited contamination of these enclaves by the host rock and conversely [57]. The presence of felsic veins within enclaves provides further evidence of magma mixing during the formation of these enclaves.

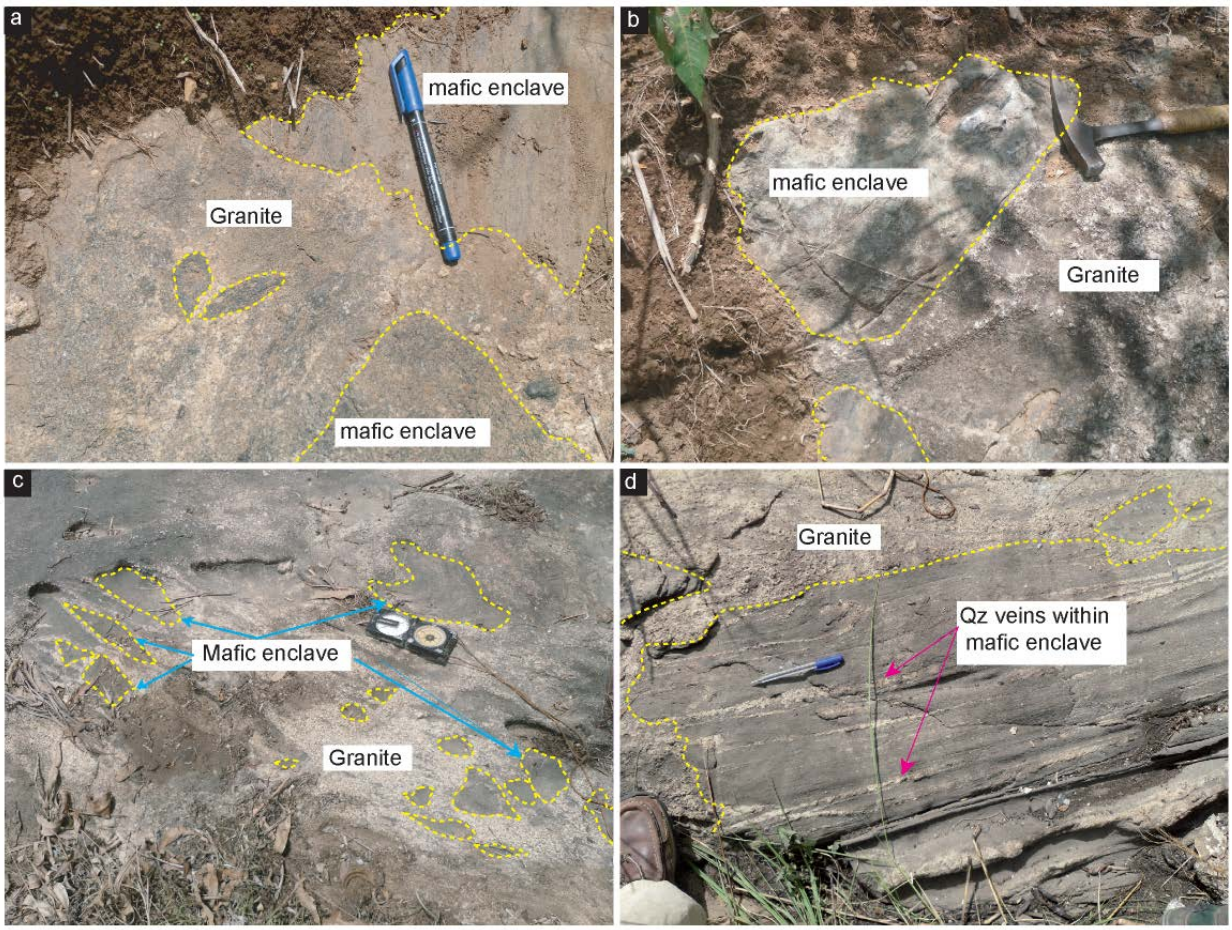

Figurer 11. Macroscopic sizes and shapes of the mafic intrusions and their relationship with the host rock

Numerous microscopic petrographic features also highlight the mixing. The reverse zoning observed in some plagioclase crystals is a disequilibrium texture that indicates magma mixing. The presence of resorption surfaces in plagioclases and corroded margins of some Amp crystals are somewhat consequences of magma mixing. This particular chemical corrosion is suggestive of disequilibrium system resulting from chemical and/or thermal changes during melting process and possibly points out magma mixing event [60]. Furthermore, the presence of acicular Ap crystals in some monzodiorites has been interpreted by [61] as suggestive of quenching occurred consequently to a mixing of a hot mafic melt with a cooler granitic magma.

Amp crystals of the granitoids are slightly richer in Fe^{3+}, Si, and Mg than those of monzodiorites. This has been used by [62] as an argument to highlight the importance of magma mixing; although the observed compositional similarity of the plagioclase and Bt phenocrysts from monzodiorites and their host granitoids indicate that the studied monzodiorites were mainly equilibrated with their hosts.

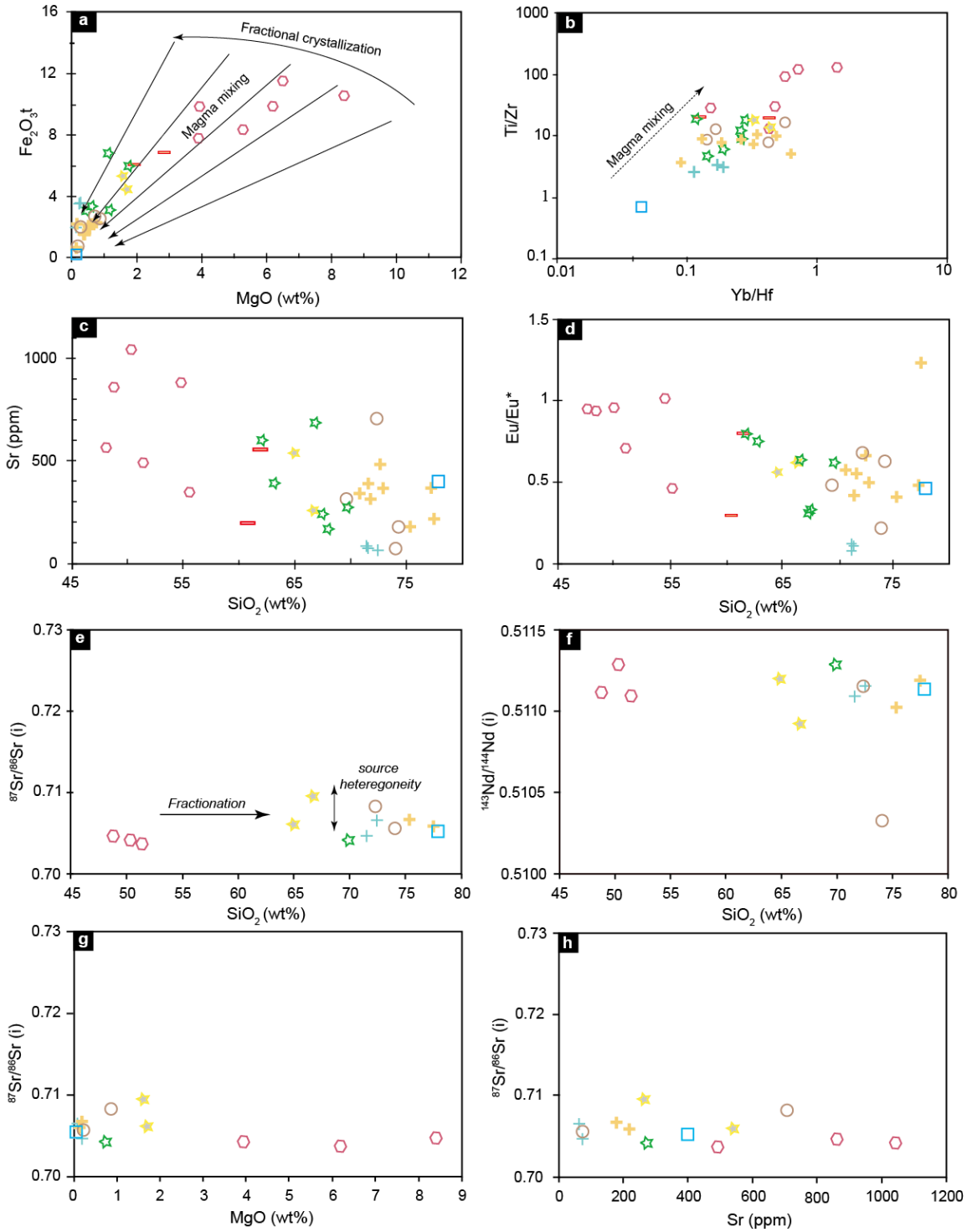

Figure 12. Geochemical and AFC discrimination diagrams of the Mbengwi plutonic rocks. (a) FeO_t vs. MgO; (b) Ti/Zr vs. Yb/Hf diagram [65] indicative magma mixing in the evolution of the studied rocks; (c) Sr vs. SiO_2; (d) Eu/Eu* vs. SiO_2; (e-f) SiO_2 vs. $^{87}Sr/^{86}Sr(i)$, $^{143}Nd/^{144}Nd(i)$; (g-h) $^{87}Sr/^{86}Sr(i)$ vs. MgO (wt%.) and Sr (ppm)

The use of the FeO -MgO diagram (Figure 12a) reveals that, the monzodiorites do not plot along the fractional crystallization trend, but rather near the mixing line as mafic end-member, while the host granitoids plot as the felsic end-member, with a reasonable linear relationship between the two that reflects a magma-mixing trend, similar to those of rocks with hybrid origin [63,64]. The role of mixing in the genesis of the Mbengwi plutonic rocks has been furthermore examined using the Yb/Hf ratio plotted against Ti/Zr (Figure 12b; e.g. [65]). The increasing linear correlations between these ratios are all features expected for magma mixing.

5.2.2. Fractional Crystallization

Fractional crystallization process is well evidenced both in the Harker diagrams and in oxides vs. MgO diagrams. Straight curves symbolize the fractionation of a constant mineralogical assemblage, while slope failures usually indicate a change in the composition of the assemblage [66]. Plots of selected major oxides and trace elements show well-defined negative or positive correlations with increasing SiO_2 content (Figure 7), which reveal fractionation of common mineral phases in the granitic magmas. Both the granitoids and monzodiorites are characterized by the decrease in MgO, CaO, Al_2O_3, and Fe_2O_{3T} contents, as well as the increase in K_2O contents, with increasing silica suggesting that fractional crystallization was dominated by Amp and calcic plagioclase. The high $(La/Yb)_N$ ratio values in granitoids (average ≈ 36) contrary to the lower ones in the monzodiorites (average ≈ 11) respectively reflect their strongly and moderately fractionated nature. The observed negative Ti anomaly is related to fractionation of Ti-bearing phases (Ilm, Spn and/or titanomagnetite), while the negative P anomaly likely results from Ap separation. According to [66], fractional crystallization could be incomplete if the residual liquid (or part of it) remained trapped within the crystal matrix. This is overall reflected in our case by the presence of a protomylonitic texture in coarse-grained granitoids marked by the presence of large phenocrysts molded by fine interstitial crystals.

The decreases of Sr contents and Eu/Eu* values with silica rising (Figure 12c-d) in addition to the depletions in Rb, K and Sr, and the general negative Eu anomalies are principally related to feldspar fractionation, particularly in felsic magmas, as Eu is highly compatible in plagioclase and K-feldspars [67]. Such negative Eu anomalies are most likely attributed to the removal of feldspar from the melt by crystal fractionation or the partial melting of a rock in which feldspar is retained in the source. Thus, the difference in the extent of the negative Eu anomalies observed within granitoids indicates that the fractionation of feldspars was more dominant in the generation of Amp+Bt-granites. One Bt-granite sample (E_{20}) displays a slight positive Eu anomaly. This sample showing a small positive Eu anomaly has the lowest LREE and HREE abundances; therefore the small positive Eu anomaly simply results from depletion of LREE and HREE through fractionation of accessory phases.

During the evolution of the studied rocks, fluids fractionation might have been an important process in regards to their average value of the Nb/Ta ratio (~17.5 in monzodiorites; ~15.2 in granitoids) according to [68].

In order to assess the role of assimilation and fractional crystallization (AFC) vs. fractional crystallization (FC) processes in the genesis of the studied rocks, Sr and Nd isotopic ratios were plotted against SiO_2, MgO and Sr (Figure 12 e-g). $^{87}Sr/^{86}Sr(i)$ and $^{143}Nd/^{144}Nd(i)$ ratios remain nearly constant with varying SiO_2 (Figure 12e-f), and the same holds true for $^{87}Sr/^{86}Sr(i)$ vs. MgO and Sr (Figure 12h-g). This indicates that the magmatic evolution of the studied rocks was mostly controlled by FC rather than AFC processes.

5.3. Geodynamic Significance

Mbengwi granitoids show many geochemical similarities such as high alkali contents and high $XFeO^T$ (≥ 0.70), low Ba and Sr contents, and pronounced Eu anomalies with various high-K syn- to post-tectonic Pan-African granitoids from many localities in Cameroon (e.g. [69]) and with Neoproterozoic transitional to calc-alkaline granitoids from NE Brazil [70].

Generally, high-K calc-alkaline granitoids are related to subduction zones, as it is the case of Pan-African granites of eastern Nigeria, emplaced during a collision-subduction of the eastern edge of the West African craton ([71] and references therein). Several works on the Central African Pan-African chain [72] suggest that it was emplaced in a subduction context (640 Ma; [19]), distinct to the granites from Nigeria that were emplaced in a continent-continent collision context at around 620±10 Ma. This subduction context of our Pan-African rocks is justified by their calc-alkaline nature, negative anomalies in Nb, light LREE-enriched patterns and weak fractionation of MREE and HREE.

6. Conclusions

Mineral chemistry and bulk-rock data of the Mbengwi Pan-African high-K calc-alkaline I-type plutonic rocks have been capitalized to investigate their petrogenetic conditions. The leading conclusions are as follows:

1. The studied plutonic rocks are enriched in LILE and depleted in HFSE. They display ΣREE-enrichment (average ≈ 366.3 ppm), and strongly LREE-fractionated patterns ($(La/Yb)_N$ ratios average ≈ 40) with an overall negative anomalies in Rb, Sr, P, Ti, Eu, and positive ones in Th and La.
2. The granitoids and monzodiorites result from partial melting of several heterogeneous protoliths relatively rich in K. The studied rocks were emplaced between 4 and 34 km deep, at pressure ranging from 1.2 to 9.4 Kbars.
3. Their differentiation might be a combined result of fractional crystallization or/and mixing (mingling) processes with negligible assimilation.

Acknowledgements

Authors acknowledge the constructive comments of anonymous reviewers and are also grateful to the editors for the diligent editorial handling of the manuscript.

References

[1] Chappell, B.W., White, A.J.R., "Two contrasting granite types: 25 years later", *Australian J Earth Sci*, 48, 489-499, 2001.

[2] King, P.L., Chappell, B.W., Allen, C.M., White, A.J.R., "Are A-type granites the high temperature felsic granites? Evidence from fractionated granites of the Wangrah suite", *Australian J Earth Sci*, 48, 501-514, 2001.

[3] Tarney, J., Jones, C.E., "Trace element geochemistry of orogenic igneous rocks and crustal growth models", *J Geol Soc*, 151 (5), 855-868, 1994.

[4] Frost, C.D., Frost, B.R., "High-K, iron-enriched rapakivi-type granites: the tholéiites connection", *Geol*, 25, 647-650, 1997.

[5] Loiselle, M.C., Wones, D.R., "Characteristics and origin of anorogenic granites", *Geol Soc Am* Abstr with Programs 11, 468, 1979.

[6] Conte, A.M., Cuccuru, S., D'Antonio, M., Naitza, S., Oggiano, G., Secchi, F., Casini, L., Cifelli, F., "The post-collisional late Variscan ferroan granites of southern Sardinia (Italy): Inferences for inhomogeneity of lower crust", *Lithos*, 294-295, 263-282, 2017.

[7] Dumort, J.C., *Notice explicative de la carte géologique de reconnaissance du Cameroun au 1/500 000*. In: Feuille Douala Ouest - direction des mines et géologie du Cameroun, 1968.

[8] Peronne, Y., *Notice explicative sur la feuille Wum-Banyo avec carte géologique de reconnaissance au 1/500.000*, Dir Mines Géol Yaoundé, Cameroun, 1969.

[9] Mbassa, B.J., Kamgang, P., Grégoire, M., Njonfang, E., Benoit, M., Itiga, Z., Duchene, S., Bessong, M., Wonkwenmendam, N.P., Ntepe, N., "Evidence of heterogeneous crustal origin for the Pan-African Mbengwi granitoids and the associated mafic intrusions (NW-Cameroon, central Africa)", *CR Geosci*, 348, 116-126, 2016.

[10] Mbassa, B.J., Njonfang, E., Grégoire, M., Itiga, Z., Kamgang, P., Benoit, M., Ndjigui, P.D., Ngwa, N.C., Nolla, J.D., "Evaluation of the mineralizing potential of the Mbengwi plutonics, Northwestern Cameroon, Central Africa", *Arab J Geosci*, 11, 657, 2018

[11] Toteu, S.F., Penaye, J., Poudjom Djomani, Y., "Geodynamic evolution of the Pan-African belt in central Africa with special reference to Cameroon", *Can J Earth Sci*, 41, 73-85, 2004.

[12] Nzenti, J.P., Barbey, P., Macaudière, J., Soba, D., "Origin and evolution of late Precambrian high-grade Yaounde gneisses", *Precamb Res*, 38, 91-109, 1988.

[13] Nédélec, A., Macaudière, J., Nzenti, J.P., Barbey, P., « Evolution structurale et métamorphique des schistes de Mbalmayo (Cameroun). Implications sur la structure de la zone mobile panafricaine d'Afrique Centrale au contact du craton du Congo », *C R Acad Sci*, (Paris), 75-80, 1986.

[14] Toteu, S.F., Van Schmus, R.W., Penaye, J., Michard, A., New U-Pb and Sm-Nd data from north-central Cameroon and its bearing on the pre- Pan-African history of central Africa, *Precamb Res*, 108, 45-73, 2001

[15] Abdelsalam, M.G., Liégeois, J.P., Stern, R.J., "The saharan metacraton", *J Afr Earth Sci*, 34, 119-136, 2002.

[16] Ngako, V., Njonfang, E., *Plates amalgamation and plate destruction, the western Gondwana history*. In: Closson D (ed) Tectonics, Belgium, 2011, 978-953.

[17] Bouyo Houketchang, M., Penaye, J., Barbey, P., Toteu, S.F., Wandji, P., "Petrology of high pressure granulite facies metapelites and metabasites from Tcholliré and Banyo regions: Geodynamic implication for the Central African fold belt (CAFB) of North-central Cameroon", *Precamb Res* 224, 412-413, 2013.

[18] Njanko, T., Nédélec, A., Affaton, P., "Syn-kinematic high-K calc-alkaline plutons associated with the Pan-African Central Cameroon shear zone (W-Tibati area): Petrology and geodynamic significance", *J Afr Earth Sci*, 44, 494-510, 2006.

[19] Ngako, V., Affaton, P., Njonfang, E., "Pan-African tectonics in northwestern Cameroon: implication for the history of western Gondwana", *Gond Res*, 14, 509-522, 2008.

[20] Toteu, S.F., Michard, A., Bertrand, J.M., Rocci, G., "U-Pb dating of Precambrian rocks from northern Cameroon, orogenic evolution and chronology of the Pan-African belt of central Africa", *Precamb Res*, 37, 71-8, 1987.

[21] Mbassa, B.J., Njonfang, E., Benoit, M., Kamgang, P., Grégoire, M., Duchene, S., Brunet, P., Ateba, B., Tchoua, F.M., "Mineralogy, geochemistry and petrogenesis of the recent magmatic formations from Mbengwi, a continental sector of the Cameroon Volcanic Line (CVL), Central Africa", *Miner Petro*, 106, 217-242, 2012.

[22] Pouchou, J.L., Pichoir, F., *Quantitative analysis of homogeneous or stratified microvolumes applying the model 'PAP'*. In: Heinrich KFJ, Newbury DE (eds) Electron probe quantitation. Plenum Press, New York, 1991, 31-75.

[23] Jochum, K.P., Weis, U., Schwager, B., Stoll, B., Wilson, S.A., Haug, G.H., Andreae, M.O., Enzweiler, J., "Reference Values Following ISO Guidelines for Frequently Requested Rock Reference Materials", *Geostand Geoanal Res*, 40(3), 333-350, 2015.

[24] Xie, X., Yan, M., Li, L., Shen, H., "Geochemical Reference Samples, Drainage Sediment GSD 1-8 from China", *Geostandards Newsletter*, 1985.

[25] Tischendorf, G., Gottesmann, B., Förster, H.-J., Trumbull, R.B., "On Li-bearing micas: estimating Li from electron microprobe analyses and an improved diagram for graphical representation", *Mineral Mag*, 61, 809-834, 1997.

[26] Tröger, W.E., *Optische Bestimmung der gesteinsbildenden Minerale. Teil 2*. Scheweizerbartsche Verlagsbuchhandlung, Stuttgart, 1982

[27] Deer, W.A., Howie, R.A., Zussman, J., *An introduction to the rock forming minerals*, 2nd ed. Springer, London, 1992.

[28] Nachit, H., Ibhi, A., Abia E.H., Ben Ohoudet, M., "Discrimination between primary magmatic biotites, reequilibrated biotites and neoformed biotites", *C R Geosci*, 337, 1415-1420, 2005.

[29] Keeditse, M., Rajesh, H.M., Belyanin, G.A., Fukuyama M., Tsunogae, "Primary magmatic amphibole in Archaean meta-pyroxenite from the central zone of the Limpopo Complex, South Africa", *S Afr J Geol*, 119 (4), 607-622, 2016.

[30] Hawthorne, F.C., Oberti, R., Harlow, G.E., Maresch, W.V., Martin, R.F., Schumacher, J.C., Welch, M., "IMA Report - Nomenclature of the amphibole supergroup", *Am Mineral* (97/11-12), 2031-2048, 2012.

[31] Smith, D.C., "Highly aluminous sphene (titanite) in natural high-pressure hydrous eclogite facies rocks from Norway and Italy, and experimental runs at high pressure", *Abst, 26th Intern Geol Conf*, Paris, 1980.

[32] Hey, M.H., "A new review of the chlorites", *Mineral Mag*, 30, 277-292, 1954.

[33] Middlemost, E.A.K., "Naming material in the magma/igneous rock system", *Earth Sci Rev*, 37, 215-224, 1994.

[34] Le Bas, M., LeMaitre, R., Streckeisen, A., Zanettin B., "A chemical classification of volcanic rocks based on the total alkali-silica diagram", *J. Petrol*, 27 (3), 745-750, 1986.

[35] Le Maître, R.W., Bateman, P., Dubek, A., Keller, J., Lameyre, J., Le Bas, M.J., Sabine, P.A., Schmid, R., Sorensen, H., Streckeisen, A., Woolley, A.R., Zanettin, B., *A classification of igneous rocks and glossary of terms. Recommendations Int Union Geol Sci Sub commission on the Systematic of Igneous rocks*, Oxford, Blackwell, 1989.

[36] Maniar, P.D., Piccoli, P.M., "Tectonic discrimination of granitoids", *Geol Soc Am Bull*, 101, 635-643, 1989.

[37] Chappell, B.W., White, A.J.R., "I- and S-type granites in the Lachlan fold belt", *Trans R Soc Edinb Earth Sci*, 83, 1-26, 1992.

[38] Frost, B.R., Arculus, R.J., Barnes, C.G., Collins, W.J., Ellis, D.J., Frost, C.D., "A geochemical classification of granitic rocks", *J Petrol*, 42, 2033-2048, 2001.

[39] Taylor, S.R., McLennan, S.M., *The Continental Crust: Its composition and evolution*, Blackwell, Oxford, 1985

[40] Anders, E., Grevesse, N., "Abundances of the elements: Meteoritic and solar", *Geochim Cosmochim Acta*, 53, 197-214, 1989.

[41] De Paolo, D.J., "Trace elements and isotopic effects of combined wallrock assimilation and fractional crystallization", *Earth Planet Sci Lett*, 53, 189-202, 1981.

[42] Roberts, M.P., Clemens, J.D., "Origin of high-potassium, calcalkaline, I-type granitoids", *Geol*, 21, 825-828, 1993.

[43] Liégeois, J.P., Black, R., Navez, J., Latouche, L., "Early and late Pan-African orogenies in the Aïr assembly of terrane (Tuareg shield, Niger)", *Precamb Res*, 67, 59-88, 1994.

[44] Barbarin, B., "Genesis of the two main types of peraluminous granitoids", *Geol*, 24, 295-298, 1996.

[45] Wones, D.R., "Significance of the assemblage titanite + magnetite + quartz in granitic rocks", *Am Miner*, 74, 744-749, 1989.

[46] Chappell, B.W., White ,A.J.R., "Two contrasting granite types", *Pacific Geol*, 8, 173-174, 1974.

[47] Martin, H., Smithies, R.H., Rapp, R., Moyen, J.F., Champion, D., "An overview of adakite, tonalite-trondhjemite-granodiorite (TTG), and sanukitoid: relationships and some implications for crustal evolution", *Lithos*, 79 (1-2), 1-24, 2005.

[48] Jiang, Y.H., Jiang, S.Y., Dai, B.Z., Liao, S.Y., Zhao, K.D., Ling, H.F., "Middle to late Jurassic felsic and mafic magmatism in southern Hunan province, southeast China: implications for a continental arc to rifting", *Lithos*, 107, 185-204, 2009.

[49] Li, Y.J., Zhao, R.F., Li, Z.C., Liu, Z.W., Li, Y., "Origin discrimination of granitoids formed by mingled magma: using a trace element diagram and exemplified by Wenquan granites, western Qinling", *J Changan Univ Earth Science* Ed, 25 (3), 7-11, 2003 (in Chinese with English abstract).

[50] Holland, T., Blundy, J., "Non-ideal interactions in calcic amphiboles and their bearing on amphibole plagioclase thermometry", *Contrib Mineral Petrol*, 116, 433-447, 1994.

[51] Blundy, J.D., Holland, T.J.B., "Calcic amphibole equilibria and a new amphibole-plagioclase geothermometer", *Contrib Mineral Petrol* 104, 208-224, 1990.

[52] Schmidt, M.W., "Amphibole composition in tonalite as a function of pressure: an experimental calibration of the Al-in-hornblende barometer", *Contrib Miner Petrol*, 110, 304-310, 1992.

[53] Anderson, J.L., Smith, D.R., "The effect of temperature and oxygen fugacity on Al-in-hornblende barometry", *Am Mineral*, 80, 549- 559, 1995.

[54] Ushida, E., Endo, S., Makino, M., "Relationship between solidification depth of granitic rocks and formation of hydrothermal ore deposits", *Resource Geology*, 57 (1), 47-56, 2007.

[55] Czamanske, G.K., Wones, D.R., "Oxidation during magmatic differentiation, Finnmarka complex, Oslo area, Norway: Part 2, the mafic silicates", *J Petrol*, 14, 349-380, 1973.

[56] Bora, S., Kumar, S., "Geochemistry of biotites and host granitoids plutons from the Proterozoic Mahakoshal Belt, central India tectonic zone: implication for nature and tectonic setting of magmatism", *Int Geol Rev*, 57, (11-12), 1686-1706, 2015

[57] Nédelec, A., Bouchez, J.L, *Pétrologie des granites, structure, cadre géologique*, Vuibert, Paris, 2011.

[58] Blundy, J.D., Sparks, R.S.J., "Petrogenesis of Mafic Inclusions in Granitoids of the Adamello Massif, Italy", J. Petrol., 33 (5), 1039-1104, 1992.

[59] Bonin, B., "Do coeval mafic and felsic magmas in postcollisional to within-plate regimes necessarily imply two constrasting, mantle and crustal sources? A review", *Lithos*, 78, 1-24, 2004.

[60] D'Lemos, R.S., "Mixing between granitic and dioritic crystal mushes, Guernsey, Channel Island, UK", *Lithos*, 38: 233-257, 1996.

[61] Vernon, R.H., "Micro-granitoid enclaves: globules of hybrid magma quenched in a plutonic environment", *Nature*, 304:438-439, 1984.

[62] Kocak, K., Zedef, V., Kansun, G., "Magma mixing/mingling in the Eocene Horoz (Nigde) granitoids, Central southern Turkey: evidence from mafic microgranular enclaves", *Miner Petrol*, 103, 149-167, 2011.

[63] Yang, H., Ge, W.C., Zhao, G.C., Dong, Y., Xu, W.L., Wang, Z.H., Ji, Z., Yu, J.J., "Late Triassic intrusive complex in the Jidong region, Jiamusi-Khanka Block, NE China: geochemistry, zircon U-Pb ages, Lu-Hf isotopes, and implications for magma mingling and mixing", *Lithos*, 224-225, 143-159, 2015.

[64] Yu, J.J., Hou, X.G., Ge, W.C., Zhang, Y.L., Liu, J.C., "Magma mixing genesis of the Early Permian Liulian pluton at the northeastern margin of the Jiamusi massif in NE China: evidences from petrography, geochronology and geochemistry", *Acta Petrol Sin*, 29 (9), 2971-2986, 2013 (in Chinese with English abstract)

[65] Aydoğan, M.S., Coban, H., Bozcu, M., Akinci, Ö., "Geochemical and mantle-like isotopic (Nd, Sr) composition of the Baklan Granite from the Muratdağı Region (Banaz, Uşak), western Turkey: Implications for input of juvenile magmas in the source domains of western Anatolia Eocene-Miocene granites", *J Asian Earth Sci*, 33, 155-176, 2008.

[66] Bonin, B., Moyen, J.F., *Magmatisme et roches magmatiques*, 3e édition, Dunod, Paris, 2011.

[67] Nash, B.P., Crecraft, H., "Partition coefficients for trace elements in silicic magmas", *Geochem Cosmochim Acta*, 49 (11), 2309-2322, 1985.

[68] Dostal, J., Chatterjee, A.K., "Contrasting behaviour of Nb/Ta and Zr/Hf ratios in a peraluminous granitic pluton (Nova Scotia, Canada)" *Chem Geol*, 163, 207 - 218, 2000.

[69] Tetsopgang, S., Suzuki, K., Njonfang, E., "Petrology and CHIME geochronology of Pan-African high K and Sr/Y granitoids in the Nkambe area, Cameroon" *Gond Res*, 14, 686-699, 2008.

[70] Guimarães, I.P., Da Silva Filho, F.A., Almeida, C.N., Van Schmus, W.R., Araujo, M.M.J., Melo, S.C., Melo, E.B., "Brasiliano (Pan-African) granitic magmatism in the Pajeù-Paraıba belt, northeast Brazil: an isotopic and geochronological approach", *Precamb Res*, 135, 23-53, 2004.

[71] Kwékam, M., *Genèse et évolution des granitoïdes calco-alcalins au cours de la tectonique panafricaine: le cas des massifs syn à tardi-tectoniques de l'Ouest-Cameroun (Régions de Dschang et de Kekem)*, Thèse Doct d'État, Univ Yaoundé I, 2005.

[72] Njonfang, E., Ngako, V., Kwékam, M., Affaton, P., « Les orthogneiss calco-alcalins de Foumban-Bankim: témoins d'une zone de cisaillement de haute température », *CR Géosci*, 338, 606-616, 2006.

[73] Smith, J.V., Brown, W.L., *Feldspar Minerals, Vol. 1: Crystal structures, physical, chemical and microstructural properties*, 2nd edn, Springer-Verlag, New York, 1988.

[74] Abdel-Rahman, A.M., "Nature of biotites from alkaline, calc-alkaline, and peraluminous magmas", *J Petrol* 35, 525-541, 1994.

[75] Whitney, D.L., Evans, B.W., "Abbreviations for names of rock-forming minerals", *American Miner*, 95, 185-187, 2010.

[76] Rickwood, P.C., "Boundary lines within petrologic diagrams which use oxides of major and minor elements", *Lithos*, 22, 247-264, 1989.

[77] McDonough, W.F., Sun, S.S., "The composition of the Earth", *Chem Geol*, 120, 223-253, 1995.

[78] Patino Douce A.E., Beard J.S., "Effects of P, f(O_2) and Mg/Fe ratio on dehydratation melting of model métagreywackes", *J Petrol*, 37, 999-1024, 1996.

[79] Singh, J., Johanneses, W., "Dehydration melting of tonalites: Part II. Composition of melts and solids", *Contrib Miner Petrol*, 125, 26-44, 1996.

[80] Altherr, R., Holl, A., Hegne, E., Lange, C., Kreuze, H, "High potassium, calc-alkaline I-type plutonism in the European Variscides: northern Vosges (France) and northern Schwarzwald (Germany)", *Lithos*, 50, 51-73, 2000.